

## Original Article

**Cite this article:** Manniello C, Agosta F, Todaro S, Cavalcante F, and Prosser G (2023) Fracture stratigraphy of Mesozoic platform carbonates, Agri Valley, southern Italy. *Geological Magazine* 159: 1874–1896. <https://doi.org/10.1017/S0016756822000322>

Received: 21 December 2021

Revised: 4 April 2022

Accepted: 5 April 2022

First published online: 19 May 2022


**Keywords:**

depositional setting; carbonate petrography; XRPD analysis; diffuse fractures; fracture density; fracture intensity; multiscale fracture distribution

**Author for correspondence:**

C. Manniello, Email: [c.manniello@unibas.it](mailto:c.manniello@unibas.it)

# Fracture stratigraphy of Mesozoic platform carbonates, Agri Valley, southern Italy

C Manniello<sup>1</sup> , F Agosta<sup>1</sup>, S Todaro<sup>2</sup>, F Cavalcante<sup>3</sup> and G Prosser<sup>1</sup>

<sup>1</sup>Department of Science, University of Basilicata, Potenza, Italy; <sup>2</sup>Department of Earth and Marine Sciences, University of Palermo, Palermo, Italy and <sup>3</sup>Institute of Methodologies for Environmental Analyses – CNR, Tito Scalo (PZ), Italy

**Abstract**

The Viggiano Mt. platform carbonates form a layered succession cross-cut by a dense array of pressure solution seams, and five sets of fractures and veins, which together form a sub-seismic structural network associated with polyphasic tectonic evolution. To assess the influence exerted by depositional and diagenetic heterogeneities on fracture geometry, distribution and multiscale properties, we present the results of stratigraphic, petrographic, mineralogical and mesoscale structural analyses conducted at the Viggiano Mountain, southern Italy. Based on rock textures and fossil associations, we documented that the Sinemurian–Pleinsbachian carbonates were deposited in a low-energy open lagoon, the Toarcian carbonates in a ramp setting rimmed by sand shoals, and the Cenomanian carbonates in a medium- to high-energy, lagoonal–tidal setting. Fracture-density (P20) and intensity (P21) values computed after circular scanline measurements show similar trends in both Sinemurian–Pleinsbachian and Toarcian carbonates, consistent with the bed and bed-package heterogeneities acting as efficient mechanical interfaces during incipient faulting. On the other hand, P20 and P21 do not show very similar variations throughout the Cenomanian carbonates due to pronounced bed amalgamation. Throughout the study area, the aforementioned parameters do not vary in proportion to the bed thickness, and show higher values within the coarse-grained carbonate beds. This conclusion is confirmed by results of linear scanline measurements, which focus on the P10 properties of the most common diffuse fracture set. The original results reported in this work are consistent with burial-related, physical–chemical compaction and cementation processes affecting the fracture stratigraphy of the Mesozoic platform carbonates.

**Highlights**

- Open-to-tidal lagoonal depositional settings of platform carbonates subjected to 4–5 km of tectonic burial.
- Depositional and diagenetic heterogeneities confining high-angle fractures.
- Varying multiscale spacing distributions in diffuse and localized fracture networks.
- Fracture density and intensity do not vary in proportion to the bed thickness.
- Greatest values of fracture density and intensity are calculated within coarse-grained carbonate beds.

**1. Introduction**

It is well known that platform carbonates deposited in lagoonal/peritidal environments often form well-layered successions (Tucker, 1985), and include low-porosity rocks (Lucia, 1983; Lucia & Fogg, 1990; Flügel, 2004) bounded by primary interfaces at the scales of single beds, bed packages and bed package associations (Moore, 2002; Spalluto, 2008, 2012; Giuffrida *et al.* 2020; La Bruna *et al.* 2020). Within low-porosity carbonates, typical of Type I fractured reservoirs (Nelson, 2001), the total amount of effective porosity is often enhanced by fractures (Odling *et al.* 1999; Korneva *et al.* 2014; Giuffrida *et al.* 2019). Fractures can occur at both micro- and mesoscale and might result confined within discrete rock intervals forming single mechanical units (Gross, 1993; Gross *et al.* 1995; Panza *et al.*, 2016, 2019; Smeraglia *et al.* 2021a). Bed-parallel pressure solution seams often localize within the primary interfaces (Rustichelli *et al.* 2012, 2015) and act as mechanical boundaries inhibiting the vertical fracture propagation (Nur & Israel, 1980; Gross *et al.* 1995, 1997; Wu & Pollard, 1995; Becker & Gross, 1996). The interaction between primary interfaces and fracture geometry and distribution is assessed by fracture stratigraphy analysis as first proposed by Berry *et al.* (1996) and subsequently refined by Laubach *et al.* (2009). Accordingly, layered rock successions are subdivided into discrete intervals according to fracture characteristics (i.e. height, spacing, density, intensity) and/or specific failure modes (Pollard & Aydin, 1990; Dershowitz & Herda, 1992; Bai & Pollard, 2000; Antonellini *et al.* 2008; Agosta *et al.* 2009, 2015).

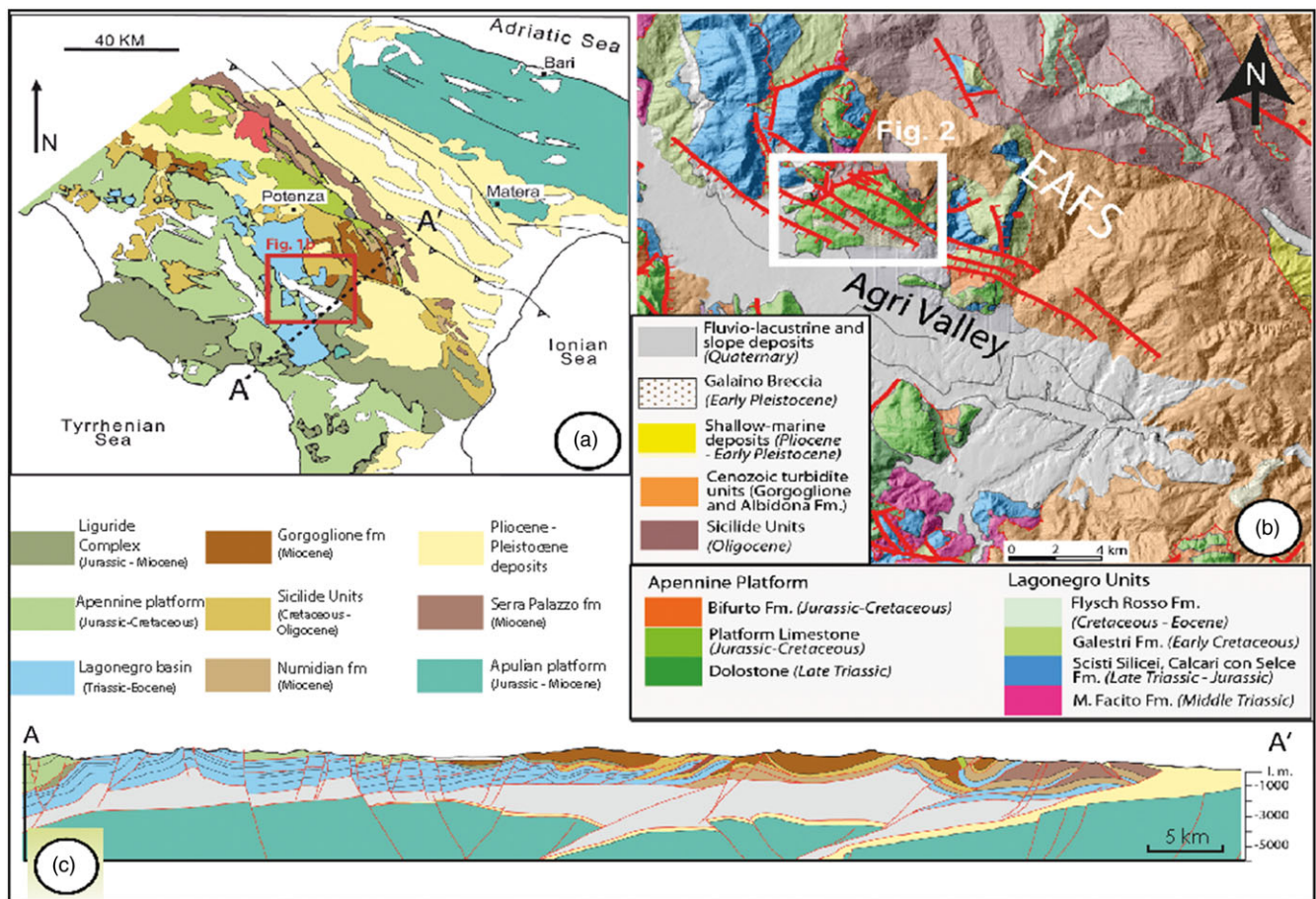


**Fig. 1.** (a) Simplified structural map of the southern Apennines fold-and-thrust belt, Italy (modified after Piedilato & Prosser, 2005). (b) Geological map of the High Agri Valley, southern Italy. The white square represents the location of the Viggianno Mountain study area. (c) Geological cross-section of the southern Apennines along the A-A' transect (modified after Prosser *et al.* 2021).

In this work, we analyse the fracture characteristics in layered Mesozoic carbonates pertaining to the Apennine Platform exposed along the axial zone of the southern Apennines fold-and-thrust belt, Italy (Patacca & Scandone, 2007; Schettino & Turco, 2011). The Mesozoic carbonates crop out at the Viggianno Mountain area (Fig. 1). Their polyphasic tectonic evolution caused the formation of multiple fracture sets forming diffuse and/or localized networks (Cello & Mazzoli, 1998; Maschio *et al.* 2005). Focusing on carbonate rock volumes mainly cross-cut by diffuse fractures, which crop out away from the major fault zones, we apply a variety of methods aimed at unravelling their stratigraphic, petrographic, mineralogical and structural properties. The results of field stratigraphic logging and petrographic and mineralogical analyses are discussed to decipher the palaeodepositional environments, diagenetic evolution and overall primary architecture of the studied Mesozoic carbonates. Also, the results of quantitative field fracture analysis are considered to assess the fracture density and intensity variations throughout the sedimentary succession. We discuss these variations in terms of the geometrical and mechanical control respectively exerted by carbonate bed thickness and carbonate rock texture on the distribution of diffuse high-angle fracture sets. Possible applications of the acquired knowledge span from groundwater management and preservation (Andreo *et al.* 2008; Marín & Andreo, 2015; Petrella *et al.* 2015; Corniello *et al.* 2018) to geothermal fluid circulation (Bellani *et al.* 2004;

Smeraglia *et al.* 2021b) and hydrocarbon production (Mosca & Wavrek, 2002; Shiner *et al.* 2004).

## 2. Geological setting

The southern Apennines of Italy extends from the southern Abruzzo – alto Molise area (Ortona – Rocca Monfina tectonic lineament; Patacca *et al.* 1990) to the Calabrian–Lucanian border (Sanginetto tectonic lineament; Amodio-Morelli *et al.* 1976). The southern Apennines are bounded westward by the Tyrrhenian back-arc extensional region (Malinverno & Ryan, 1986; Kastens & Masche 1990; Patacca *et al.* 1992a, 1992b), and eastward by the Bradanic Trough including Plio-Pleistocene foredeep basinal sedimentary successions (Patacca *et al.* 1990; Patacca & Scandone, 2007). The structural setting of the southern Apennines consists of E-to-NE-vergent thrust sheets forming a multi-duplex emplaced since the late Oligocene – early Miocene due to combined thin- and thick-skinned tectonics (Mostardini & Merlini, 1986; Casero *et al.* 1988, 1991; Monaco *et al.* 1998; Improta *et al.* 2000; Noguera & Rea, 2000; Shiner *et al.* 2004). Since the Pliocene, this multi-duplex has been dissected by transtensional and extensional faults (Mostardini & Merlini, 1986; Hippolyte *et al.* 1995; Giano *et al.* 2000; Cello *et al.* 2003; Novellino *et al.* 2015) associated with the Tyrrhenian Basin opening and/or with the gravitational collapse of the orogen (Doglioni *et al.* 1996; Cello & Mazzoli, 1998; Scrocca *et al.* 2005).

At a regional scale, the Apennine carbonate platform now forms a main thrust sheet encompassed between upper Ligurian/Sicilian and lower Lagonegro tectonic units (Vezzani *et al.* 2010, and references therein). During the Mesozoic, this carbonate platform developed along the western portion of the Jurassic Ligurian Tethys Ocean (Patacca & Scandone, 2007; Schettino & Turco, 2011) and included the following three main stratigraphic units (Patacca & Scandone, 2007):

- (1) Capri–Bulgheria, representing the westernmost portion of the ancient carbonate platform: It included Triassic–Jurassic, shallow-water, internal transitional carbonate facies and Cretaceous–Miocene marls interbedded with resedimented carbonates.
- (2) Alburno–Cervati, the ancient platform-interior portion. It contained open Triassic dolomites and dolomitic limestones, Jurassic–Cretaceous shallow-water limestones and Miocene slope carbonates and terrigenous deposits.
- (3) Maddalena Mountain, the easternmost portion of the ancient platform. It was made up of transitional facies deposited between the Alburno–Cervati Unit to the west and the Lagonegro Basin to the east.

### 2.a. Viggiano Mountain area

The Viggiano Mountain is located along the NE margin of the High Agri Valley, which is an intra-mountain tectonic basin filled with Quaternary fluvio-lacustrine deposits (Di Niro *et al.* 1992). The WNW–ESE elongated High Agri Valley basin is bounded by high-angle transtensional faults forming the East Agri Valley fault system (EAFS; Fig. 1b) and the Monti della Maddalena fault system (Cello & Mazzoli, 1998; Cello *et al.* 2000, 2003; Maschio *et al.* 2005; Prosser *et al.* 2021). The studied Mesozoic carbonates of the Viggiano Mountain are cross-cut by faults pertaining to EAFS. According to Cello & Mazzoli (1998) and Cello *et al.* (2000), the EAFS includes N120E (left-lateral slip), N30E (right-lateral transtensional slip), N90–110E (left-lateral transtensional slip) and N130–150E (left-lateral transpressional slip) high-angle fault sets. Differently, Maschio *et al.* (2005) documented left-lateral transtensional slip along WNW–ESE-striking, left-stepping master faults, and localized dilation within the releasing jogs of interacting WNW–ESE faults due to NE–SW-striking normal faults. High-angle faulting involved slope deposits and palaeosoils 39 and 18 ka old, respectively (Giano *et al.* 2000), and caused historical seismicity in the whole Agri Valley area (Mallet, 1862; Cello *et al.* 2003, Buttinelli *et al.* 2016; Hager *et al.* 2021).

According to the latest geological map available for the study area (G Palladino *et al.* in prep.), the Viggiano Mountain carbonates are bounded northward and southward by WNW–ESE-striking, high-angle transtensional faults, and westward and eastward by NE–SW-striking, high-angle extensional faults (Fig. 2a). The high-angle faults dissect the buried, NE-verging, low-angle thrust juxtaposing the Viggiano carbonates against the Lagonegro II Unit (Patacca & Scandone, 2007; Bruno *et al.*, 2014), and the associated anticline forelimb. The bottom portion of the Viggiano carbonates includes Triassic dolostones, lower Jurassic wackestones and packstones, with thick-shelled bivalve (*Lithiotis*), green algae (*Palaeodasycladus mediterraneus*) and foraminifera (*Siphoalvulina sp.*, *Pseudocyclammia liassica*) marking the Pleinsbachian age (Lechler *et al.* 2012). These carbonates formed in a subtropical, inner platform depositional environment, and were topped by thick, massive oolites postdating the Early Toarcian Anoxic event (Wignall & Bond, 2008; Trecalli *et al.*,

2012; Caruthers *et al.*, 2013). The upper portion of the Viggiano carbonates consists of Albian–Cenomanian rudstones and grainstones with gastropods, bivalves, rudists (*Radiolitidae*) and foraminifera (Lechler *et al.* 2012). The topmost carbonate beds are made up of mudstones-to-rudstones and boundstones (*Lithocodium*) with geopetal structures and rudists (*Conicorbitolina conica*, *Salpingoporella turrida* and *Caprinidae*).

### 3. Methods

The present study focuses on two main sites labelled as ‘Scarrone la macchia’ (40° 22.484′ N, 15° 50.383′ E) and ‘Il monte’ (40° 22.678′ N, 15° 51.693′ E), which are respectively located along the southern cliff (Fig. 2b) and upper portion of the Viggiano Mountain (Fig. 2c).

#### 3.a. Stratigraphic analysis and rock sampling

Field stratigraphic logging was performed aiming at assessing both bed thickness and carbonate lithofacies (Dunham, 1962). The bed thickness was measured orthogonal to laterally continuous bed interfaces. The carbonate lithofacies were characterized by means of a portable magnifying lens. A total of 70 samples were collected at the Scarrone la macchia site, and 51 samples at the Il monte site. Regarding the former, ten samples derive from outcrops exposing the bottommost portion of the oolitic carbonates and the associated primary interfaces.

#### 3.b. Petrographic analysis

The analysis was carried out using an optical microscope (Leitz Laborlux 12 Pol) associated with the Zen software for photomicrograph acquisitions. Microfacies textural classifications are after Dunham (1962) and Embry & Klovan (1971). A total of 19 thin-sections obtained from samples collected at the Scarrone la macchia and 14 at the Il monte sites were analysed. Biostratigraphic analysis of the Lower Jurassic carbonates was based on biozonal schemes and chronostratigraphic references related to the Tethyan inner-carbonate platforms (De Castro, 1991; Chiocchini *et al.*, 1994; Barattolo & Romano, 2005; BouDagher-Fadel, 2008). Biostratigraphic analysis of the Cretaceous carbonates is after the distribution ranges already described for the Tethyan realm (Chiocchini *et al.*, 1994; Di Stefano & Ruberti, 2000).

#### 3.c. Mineralogical analysis

Twenty powders obtained from the hand samples collected at the bottommost portion of the oolitic carbonates exposed at the Scarrone la macchia site were investigated. X-ray powder diffraction (XRPD) analysis was carried out by means of the Rigaku D/Max 2200 diffractometer with  $\theta$ – $\theta$  Bragg–Bentrano geometry, equipped with CuK $\alpha$  radiation, automatic sample holder spinner, secondary graphite monochromator and scintillation detector. The following instrumental conditions were adopted: (i) power 40 mA  $\times$  30 kV, (ii) step scan 0.02°  $\theta$ , (iii) speed 3s/step, (iv) divergent slit 1° and receiver slit 0.3 mm. Random powders and oriented specimens were respectively analysed in the angular range of 2–70°  $\theta$  and 2–32°  $\theta$ . Mineralogical analyses were performed on bulk samples, on their terrigenous components and on the <2  $\mu$ m terrigenous fraction (Table 1).

Hand samples were first crushed, then one aliquot was pulverized by friction in a concentric-disc agate mill, whereas another aliquot was treated with diluted HCl to first remove the carbonates



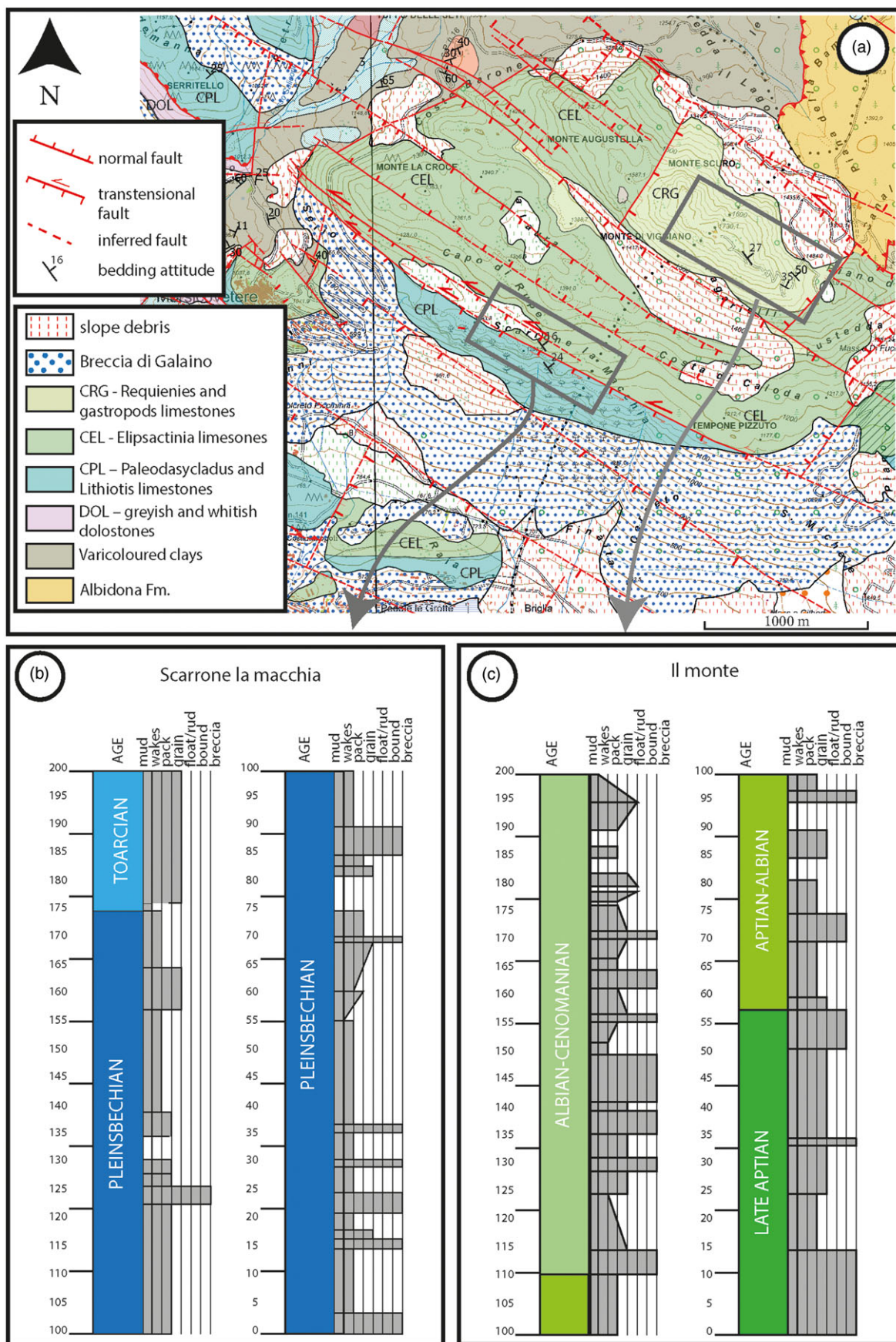


**Fig. 2.** (a) Geological map of the Viggiano Mountain area, located along the northern edge of the High Agri Valley (G Palladino *et al.* in prep.). Location of both Scarrone la macchia and Il monte study sites is reported. (b, c) Schematic stratigraphic logs of (b) Scarrone la macchia and (v) Il monte areas (modified after Lechler *et al.* 2012).

**Table 1.** Sample code, lithology, components and fractions determined by XRPD on samples collected from the Scarrone la Macchia stratigraphic section

Sample	Lithology	Random powder of bulk sample	Random powder of terrigenous component	Oriented specimens (<2 µm fraction) of the terrigenous component
O-2	Cohesive limestone	X	n.d.	n.d.
SC1	Interbed with terrigenous component	X	X	X
SC2	Interbed with terrigenous component	X	X	X
MC1	Cohesive limestone	X	X	X
MC3	Cohesive limestone	X	X	n.d.
SL2B-C1	Interbed with terrigenous component	X	X	X
SL2B-C2	Interbed with terrigenous component	X	X	X
MC4	Cohesive limestone	X	X	X
SC3	Interbed with terrigenous component	X	X	X
MC5	Cohesive limestone	X	n.d.	n.d.
MC6	Cohesive limestone	X	X	X
SC4	Interbed with terrigenous component	X	X	X
MC7	Cohesive limestone	X	X	X
A7	Cohesive limestone	X	X	n.d.
SC5	Interbed with terrigenous component	X	X	X
C1	Cohesive limestone	X	X	n.d.
D5	Cohesive limestone	X	X	n.d.
D4	Cohesive limestone	X	X	n.d.
SC6	Interbed with terrigenous component	X	X	X
D2	Cohesive limestone	X	X	X

Note: n.d., not detected because it is present in very small quantities.

(Cuadros & Altaner, 1998). The remaining silicate component was washed several times with distilled water and then collected by centrifugation. About 0.5 g of the collected silicates was manually milled using mortar and pestle, and then used for random specimen analyses by means of side loading. Also, c. 1.5 g of the collected silicates were used for clay fraction (<2 µm) separation according to Stock's law. The clay fraction was then saturated with 1N MgCl<sub>2</sub> solution and finally used for orientated specimen analysis by settling it on a glass slide (Moore & Reynolds, 1997). The oriented specimens were air-dried, ethylene glycol solvated and then heated at 375 °C (Moore & Reynolds, 1997).

### 3.d. Structural analysis

Field structural analyses were carried out by means of circular and linear scanline methods (Priest & Hudson, 1981; Mauldon *et al.* 2001). The former consisted of circles drawn on the rock surface delimiting a circular window (symmetric sampling area), in which the number of fracture intersections, *n*, and the number of fracture endpoints inside the sampling area, *m*, were measured. All fracture traces longer than 3 cm were considered. Outcrops were chosen based on accessibility, dimensions (width > 10 m) and distance

from main fault zones. The measured *m* and *n* values were respectively employed for 2D fracture density (P20) and intensity (P21) calculations (Mauldon *et al.* 2001).

P20 represents the number of fracture trace centres per unit area (1/m<sup>2</sup>), and is obtained by applying the following equation:

$$P20 = m/2\pi r$$

where *r* is the radius of the circular scanline.

P21 represents the mean total trace length of fractures per unit area (m/m<sup>2</sup>), and is obtained by applying the following equation:

$$P21 = n/4r$$

Eighty-five circular scanlines were conducted within single carbonate beds. According to the bed thicknesses, the diameter of the circular scanline varied between 15 and 50 cm. In order to obtain representative P20 and P21 estimations, circular scanlines included at least 30 endpoints (Rohrbaugh *et al.* 2002).

Thirteen linear scanline analyses were performed by considering ideal lines drawn on the rock and measuring both the attitude

and distance from origin of all surveyed fractures. As a result, true fracture spacing values ( $S_r$ ) were computed for single fracture sets. Computations were performed by applying trigonometric corrections to the apparent spacing values ( $S_a$ ) in light of the  $\alpha$  and  $\beta$  values ( $\alpha$ : azimuthal angle formed by fracture strike direction and scanline trend;  $\beta$ : zenithal angle formed by fracture dip angle and scanline plunge).

True fracture spacing is obtained by applying the following equation:

$$S_r = S_a * (\cos \alpha) * (\cos \beta)$$

At both sites, ten of the aforementioned linear scanlines were positioned parallel to carbonate beds, away from mesoscale faults, to measure the 1D fracture intensity, P10, of the high-angle WNW–ESE (Scarrone la macchia) and WSW–ENE (Il monte) fracture sets. The three other linear scanlines, respectively labelled S1 to S3, were performed along orthogonal outcrops of the Scarrone la macchia site to assess the multiscale spacing distribution of the outcropping, high-angle fracture sets. Both S1 (N230E/40°) and S3 (N100E/31°) were positioned away from mesoscale faults, whereas the S2 (N180E/25°) was located across a c. N110E-striking, high-angle transtensional fault.

## 4. Results

In this chapter, we first present the stratigraphic, petrographic and mineralogical data. Then we document the geometry, density, intensity and multiscale spacing distribution of the surveyed fracture sets.

### 4.a. Carbonate stratigraphy

#### 4.a.1. Scarrone la macchia site

The c. 56 m thick succession includes two informal units (Fig. 3). The lower one is made up of well-layered carbonates with dark limestones and marly intercalations. The carbonates show a total thickness of c. 43 m (Fig. 3a) and dip NE (Fig. 3c). They are subdivided into 12 single bed packages, respectively labelled A to N bottom up, whose thickness varies from c. 13 m (bottom) to c. 1 m (top) (Fig. 3b). Single bed packages show fining-upwards carbonate textures, with thick beds of coarse-grained limestones at the bottom, and thin beds of fine-grained limestones at the top. The bed packages are bounded by laterally continuous, 5–10 cm thick, clay-rich carbonate interfaces including anastomosed pressure solution seams. Single carbonate beds are delimited by mm- to cm-thick bed interfaces, which might include pressure solution seams with siliciclastic films of insoluble material.

The well-layered carbonates are topped by an up to 15 cm thick, clay-rich carbonate layer including mm- to cm-sized elongated carbonate clasts embedded in a fine-grained matrix. The outcropping 13 m thick oolitic grainstones above mainly dip NE (Fig. 3c), forming a large-scale, open syncline. The outcropping oolitic unit at the Scarrone la macchia includes four main bed packages, respectively labelled O to R (Fig. 3a, b), delimited by laterally continuous, mm-thick, clay-rich carbonate interfaces. The single 5–40 cm thick carbonate grainstone beds show a pronounced amalgamation and significant lateral thickness variations. Bed interfaces are marked by localized pressure solution seams. At a close view, the single pressure solution seams do not show any visible insoluble clayish material.

#### 4.a.2. Il monte site

The 67 m thick massive carbonates dip NE and include 11 bed packages labelled A to M bottom up (Fig. 3d, f). The bed packages are delimited by laterally continuous, erosive surfaces, and show fining-upward trends characterized by carbonate breccia and bioclastic rudstone/floatstone at the bottom, and carbonate grainstones and/or mudstone at the top (Fig. 3e). Single carbonate breccia and rudstone/floatstone beds include rudist fragments. Bed interfaces show a very pronounced amalgamation and the presence of pressure solution seams with tabular shapes.

### 4.b. Carbonate petrography

#### 4.b.1. 'Scarrone la macchia' site

The well-layered carbonates include abundant benthic foraminifera and calcareous algae (including *Haurania* sp., *Siphovalvulina* sp., *Lituosepta* sp., *Palaeodasycladus mediterraneus* and *Thaumatoporella parvovesiculifera* (Fig. 4a–e)). Microfractures are partially occluded by blocky cement (Fig. 4g).

The oolitic limestones are made up of ooids with obliteration of the laminae due to intense micritization (Fig. 4f). However, in some cases, the original fabric consisting of concentric laminae is preserved. Ooids are 500–1000  $\mu$ m in size, cemented with blocky calcite, and consist of alternations of laminae (<1 cm thick) including micrite oncoids (>1 mm). Their nuclei are made up of skeletal grains, peloids and rare mineral grains. Suture-like contacts among grains are absent, while microfractures are visible (Fig. 4h).

#### 4.b.2. Il monte site

The massive carbonates include rudist fragments, gastropods, algae and benthic foraminifers (*Orbitolinids*) (Fig. 5a, b, c, e). Single rudist fragments, up to c. 5 cm in size, are micritized and affected by both microboring (cf. Fig. 5b) and pervasive dissolution (Fig. 5e–f). Rare stromatolitic laminae associated with oncoids and ostracods are also documented (Fig. 5d). Both granular and meniscus cements and isopachous crusts are present (Fig. 5e, f). Intergranular pores are filled with carbonate cements, barren silts and ostracod-rich sediments (Fig. 5e, f).

### 4.c. Mineralogical analysis

The results of the XRPD qualitative analyses are reported in Table 2 and Figures 6 and 7. Random powder analysis of the bulk rocks shows that all samples mainly include calcite (Fig. 6a). The silicates include quartz, feldspars (plagioclase), goethite and clay minerals such as illite, mixed-layer illite/smectite (I/S), chlorite and kaolinite (Fig. 6b). Mixed layers show ordered R1 with 80 % of illite, and R3 with 90 % of illite (Fig. 7; Table 2).

### 4.d. Structural analysis: fracture orientation

The cumulative plots of fracture poles are shown in equal-area, lower-hemisphere projections (Allmendinger *et al.* 2011) as present-day data (Fig. 8a) and after bedding restoration (Fig. 8b). Fracture data were restored by considering the attitude of single carbonate beds. The fracture poles mainly cluster around N199E/06 and N195E/23 (trend/plunge), which are related to c. WNW–ESE-striking fractures respectively dipping 84° and 67°.

In order to precisely document the fracture orientation, the available data are subdivided into three different subsets respectively corresponding to the well-layered, oolitic and massive



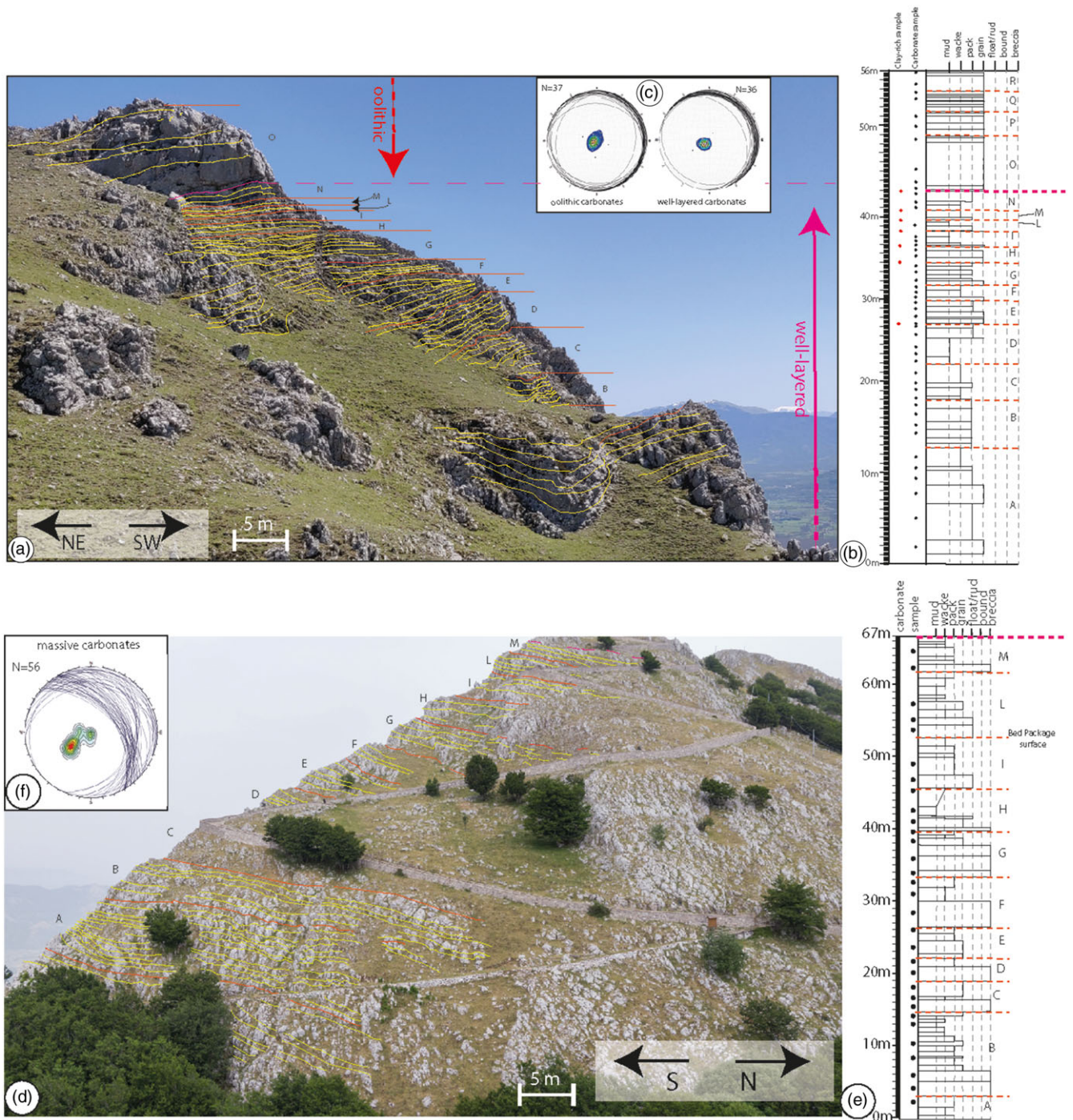


**Fig. 3.** (a) Panoramic view of the Scarrone la macchia site. Bedding surfaces (yellow lines), bed package interfaces (orange lines) and sedimentary unit interfaces (magenta line) are reported. (b) Stratigraphic log of the Scarrone la macchia site. The aforementioned interfaces are also reported. (c) Lower-hemisphere, equal-area stereographic projection of bedding planes measured in well-layered carbonates and oolitic carbonates. (d) Panoramic view of the Il monte site. Bedding surfaces (yellow dashed lines), bed package interfaces (orange lines) and sedimentary unit interfaces (magenta line) are highlighted. (e) Stratigraphic section of Il monte site. The aforementioned interfaces are also reported. (f) Lower-hemisphere, equal-area stereographic projection of bedding planes measured in the massive carbonates.

carbonates. Five main high-angle sets are shown by both original and restored data (Fig. 9):

- fractures striking WNW–ESE;
- fractures striking WSW–ENE;
- fractures striking N–S;
- fractures striking NW–SE;

- fractures striking NE–SW.

The WNW–ESE-striking fractures show a dense pole cluster in the well-layered carbonates, forming a  $68^\circ$  cut-off angle with bedding. They are also present in the oolitic carbonates, determining a  $56^\circ$  cut-off angle. The WSW–ENE-striking fractures are mainly present in the massive carbonates, forming a *c.*  $70^\circ$



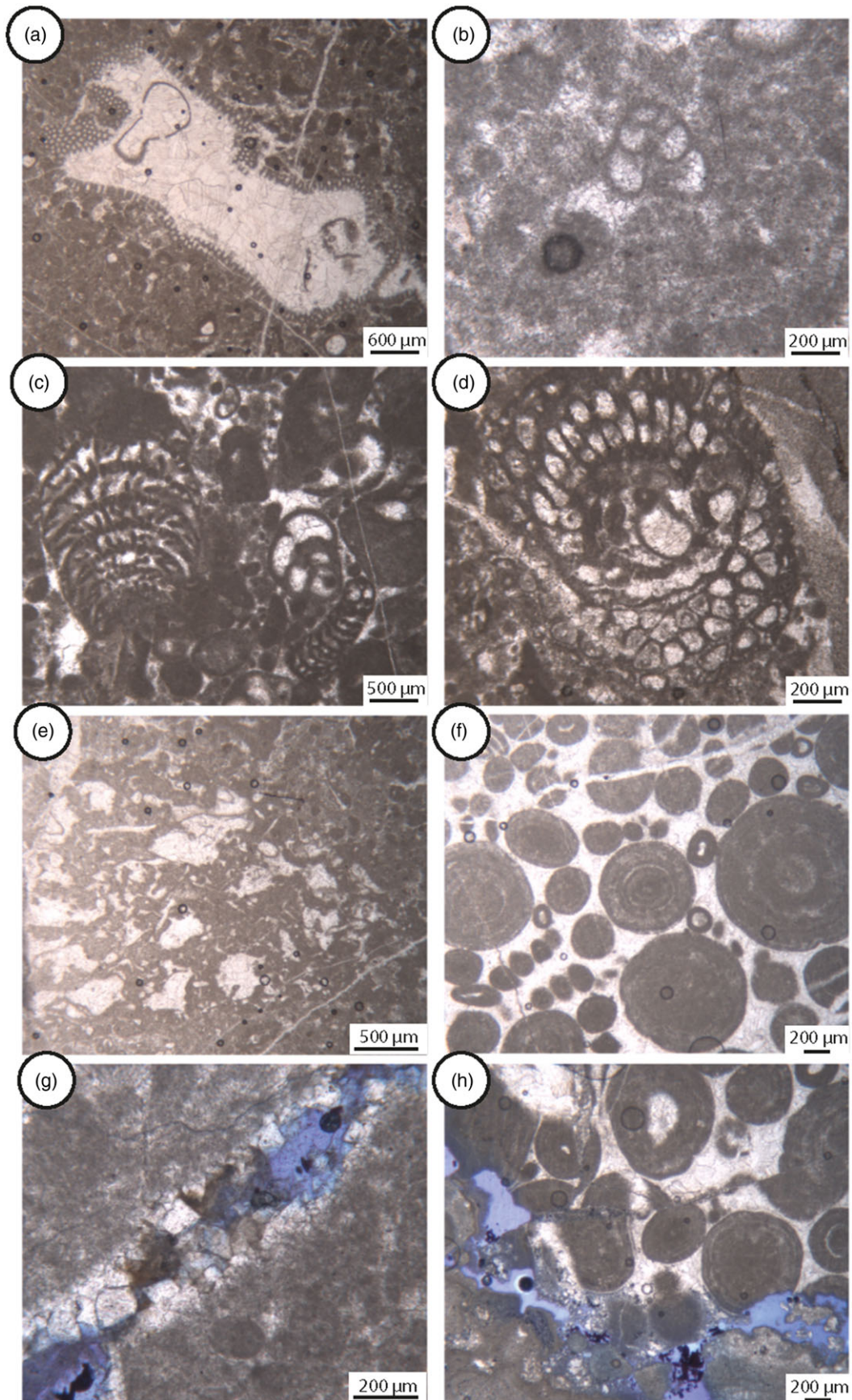


**Fig. 4.** Microfacies of the Scarrone la macchia: (a–e) well-layered carbonates, (f–h) oolitic carbonates. (a) Packstone with *Thaumatoporella parvovesiculifera*. (b) Grainstone–packstone with *Siphonalvulina* sp. (c) Grainstone–packstone with benthic foraminifera (*Siphonalvulina* sp., *Haurania deserta*, *Lituosepta* sp.). (d) *Palaeodasycladus mediterraneus*. (e) *Bacinella-Lithocodium* agregatum. (f) Oolitic grainstone. (g) Open fractures partially occluded by dolomitic cements. (h) Intergranular porosity.



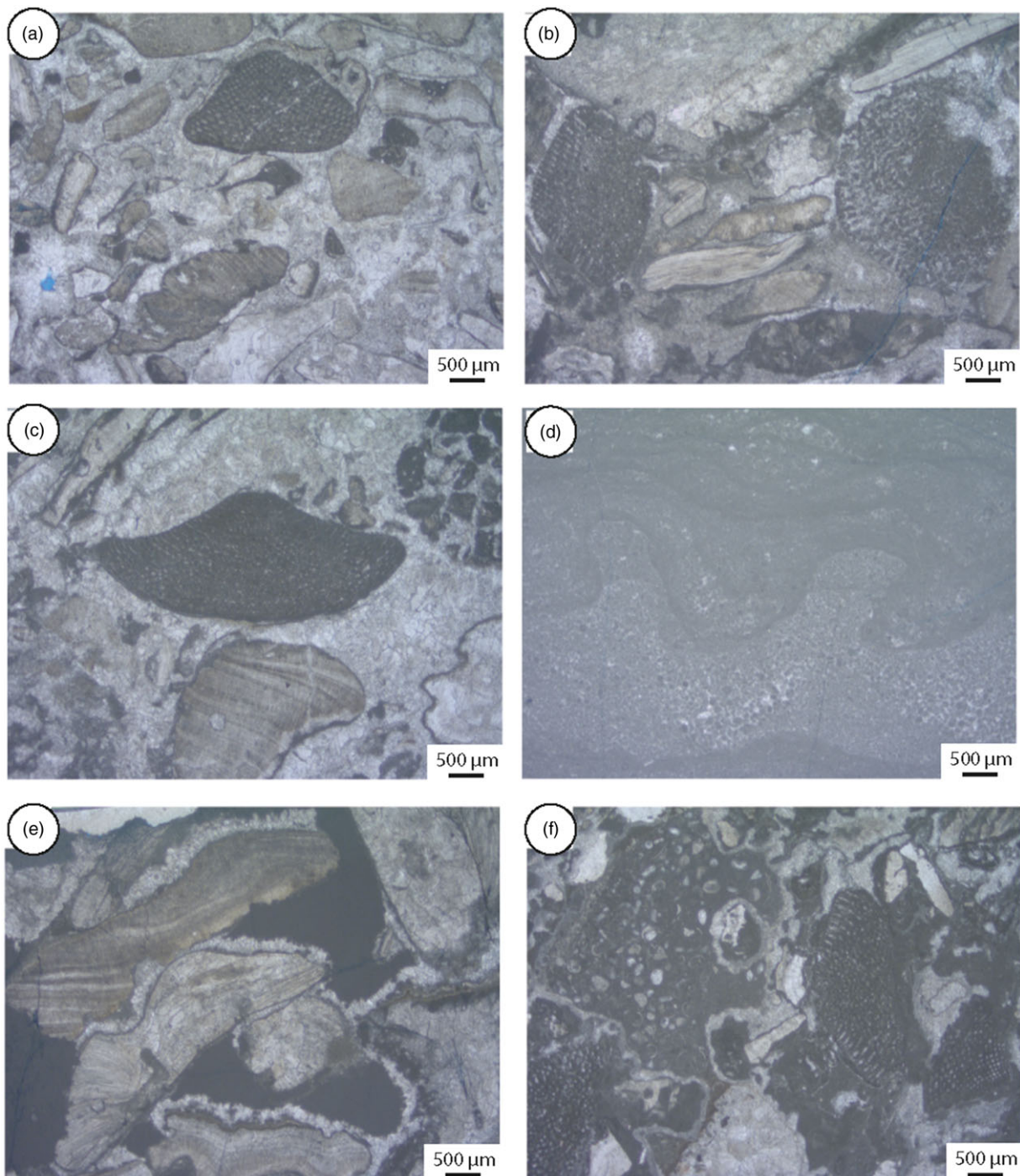


**Fig. 5.** Microfacies of the Il monte section. (a–c) Grainstone to rudstone with fragments of rudists shell, orbitolinids. (d) Stromatolitic laminae with peloids. (e) Meniscus cements connecting the grains and isopalous cements rims around the rudists fragments. Barren silt filled the residual cavities. (f) Meniscus cements connecting the grains. The residual cavity is filled by a silt rich in ostracods.

cut-off angle with bedding. The N–S-striking fractures are rare in both well-layered and massive carbonates, whereas they form a dense pole cluster in the oolitic carbonates determining a *c.* 70° cut-off angle with bedding. The NW–SE-striking fractures form low-density pole clusters in all study carbonates, with cut-off angles of 74° (well-layered carbonates) to 55° with bedding (both oolitic and massive carbonates). The NE–SW-striking fractures form low-density pole clusters in all study

carbonates, with cut-off angles of 86° (well-layered carbonates), 71° (massive carbonates) and 67° with bedding (oolithic carbonates), respectively.

#### 4.e. Structural analysis: fracture density and intensity

At the Scarrone la macchia site, (Figs 10a, 11) P20 varies from 61 m<sup>-2</sup> (1 m thick carbonate wackestone bed, *c.* 35 m above the base level) to

**Table 2.** Mineralogical assemblages of the study samples

Sample	Random powder analysis of bulk sample and terrigenous component								Oriented specimens (<2 μm)			
	Cal	Qtz	Fs	Gth	I/S	Ill	Chl	Kao	I/S features			
									Ordering, R		Illite percentage	
O-2	X	n.d.	n.d.	n.d.	n.d.	n.d.	n.d.	n.d.	n.d.	n.d.	n.d.	n.d.
SC1	X	n.d.	X	n.d.	X	X	X	n.d.	R1	R3	82	89
SC2	X	n.d.	X	n.d.	X	X	X	n.d.	n.d.	R3	n.d.	87
MC1	X	n.d.	X	n.d.	X	X	X	n.d.	n.d.	R3	n.d.	87
MC3	X	X	X	n.d.	X	X	X	n.d.	n.d.	n.d.	n.d.	n.d.
SL2B-C1	X	X	X	n.d.	X	X	X	n.d.	R1	R3	80	90
SL2B-C2	X	X	X	n.d.	X	X	X	n.d.	R1	R3	78	90
MC4	X	X	X	n.d.	X	X	X	n.d.	n.d.	R3	n.d.	87
SC3	X	n.d.	X	n.d.	X	X	X	X	n.d.	R3	n.d.	86
MC5	X	X	n.d.	n.d.	n.d.	n.d.	n.d.	n.d.	n.d.	n.d.	n.d.	n.d.
MC6	X	X	X	n.d.	X	X	X	X	R1	R3	82	89
SC4	X	n.d.	X	X	X	X	X	n.d.	R1	R3	80	89
MC7	X	X	X	X	X	X	X	n.d.	n.d.	R3	n.d.	85
A7	X	X	X	n.d.	X	X	X	n.d.	n.d.	n.d.	n.d.	n.d.
SC5	X	n.d.	X	X	X	X	X	n.d.	n.d.	n.d.	n.d.	n.d.
C1	X	n.d.	X	n.d.	X	X	X	n.d.	n.d.	n.d.	n.d.	n.d.
D5	X	X	X	n.d.	X	X	X	n.d.	n.d.	n.d.	n.d.	n.d.
D4	X	X	X	n.d.	X	X	X	n.d.	n.d.	n.d.	n.d.	n.d.
SC6	X	X	X	X	X	X	X	n.d.	n.d.	R3	n.d.	86
D2	X	n.d.	X	n.d.	X	X	X	n.d.	n.d.	R3	n.d.	87

Note: Cal, calcite; Chl, chlorite; Qtz, quartz; Fs, feldspars; Gth, goethite; I/S, mixed layers illite-smectite; Ill, illite; Kao, kaolinite. n.d., not detected; X indicates the presence of mineral phase.

552 m<sup>-2</sup> (40 cm thick carbonate packstone bed, c. 14 m above the base level) throughout the well-layered carbonates. There, P20 commonly decreases upward within single bed packages. In the same carbonate unit, P21 varies from 10 m<sup>-1</sup> (1 m-thick carbonate wackestone bed, c. 35 m above the base level) to 46.7 m<sup>-1</sup> (1.6 m thick carbonate grainstone bed, c. 7 m above the base level). Similar to fracture density, P21 also decreases upward within single bed packages.

In the oolitic carbonates (Fig. 10a), P20 varies from 87.6 m<sup>-2</sup> (90 cm thick carbonate grainstone bed, c. 55 m above the base level) to 488 m<sup>-2</sup> (50 cm thick carbonate grainstone bed, c. 50 m above the base level). P21 ranges from 1.0 m<sup>-1</sup> (90 cm thick carbonate grainstone bed, c. 55 m above the base level) to 47.5 m<sup>-1</sup> (50 cm thick carbonate grainstone bed, c. 50 m above the base level). The highest values of both P20 and P21 characterize the topmost beds of single bed packages.

The P10 values computed for the WNW–ESE and WSW–ENE-striking, high-angle fractures respectively associated with the denser pole clusters documented within the well-layered and massive carbonates are between c. 0.3 and 1.8 m<sup>-1</sup> (Table 3).

At the Il monte site (Figs 10b, 11), the massive carbonates show P20 varying from 43.3 m<sup>-2</sup> (20 cm-thick mudstone bed,

c. 14 m above the base level) to 184 m<sup>-2</sup> (3 m thick carbonate breccia bed, c. 4 m above the base level). There, P21 ranges from 8 m<sup>-1</sup> (60 cm thick carbonate packstone bed, c. 51 m above the base level) to 25 m<sup>-1</sup> (2 m thick carbonate breccia bed, c. 14 m above the base level).

#### 4.e. Structural analysis: multiscale fracture spacing properties

The fracture poles obtained after S1, S2 and S3 linear scanline measurements (Fig. 12) are reported in equal-area, lower-hemisphere projections (Fig. 13a, d, g). Along S1, the two main fracture sets respectively striking N292E and N300E show an exponential best fit ( $R^2 = 0.97$ ) and a power law best fit ( $R^2 = 0.93$ ) in the bilogarithmic fracture spacing vs cumulative number plots (Fig. 13b, c). Along S2, the two main fracture sets striking N252E and N284E are respectively characterized by power law ( $R^2 = 0.96$ ) and exponential ( $R^2 = 0.93$ ) fracture spacing distributions (Fig. 13e, f). Along S3, the two main fracture sets striking N180E and N206E respectively show power law ( $R^2 = 0.92$ ) and exponential ( $R^2 = 0.87$ ) fracture spacing distributions (Fig. 13h, i).



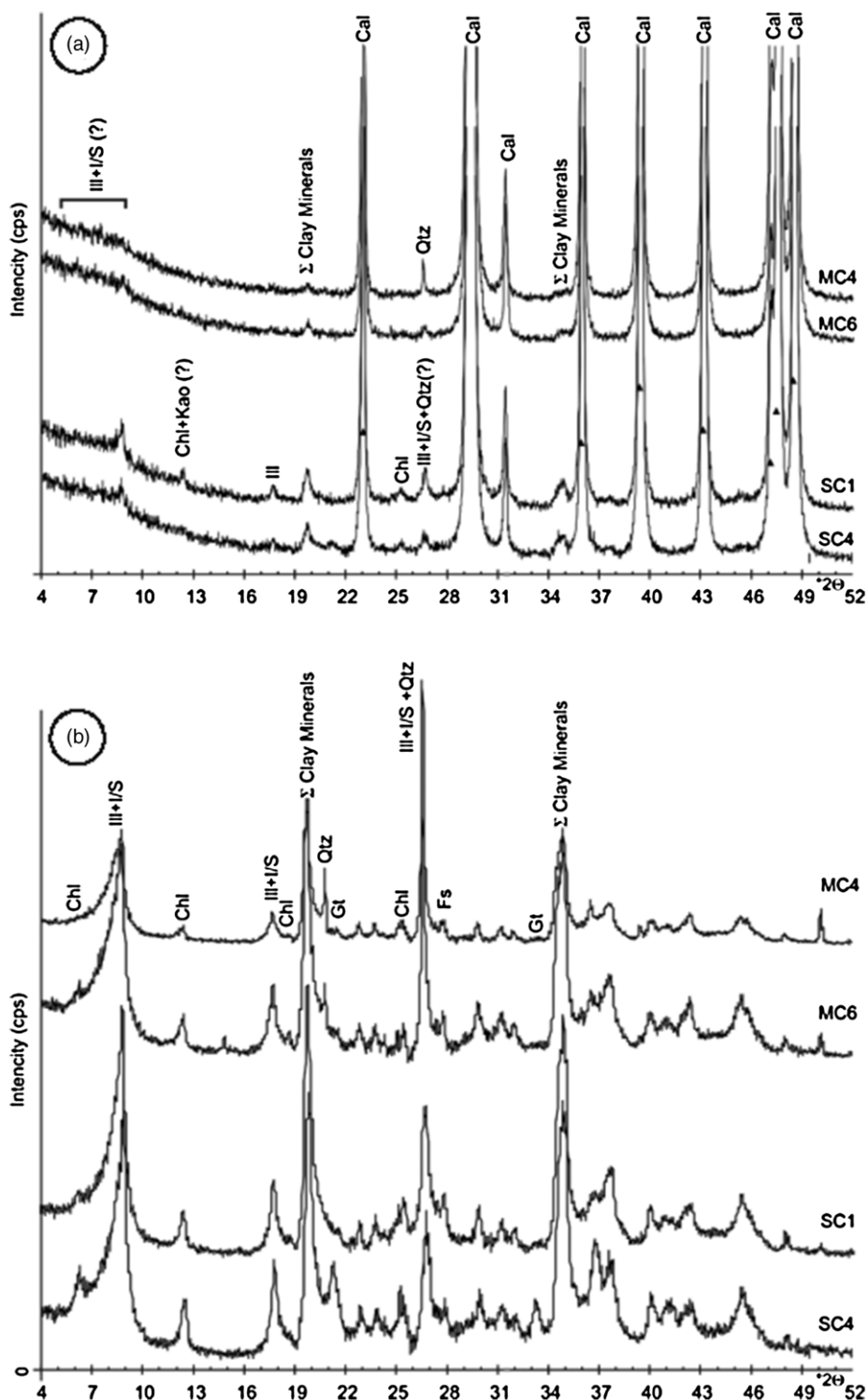


**Fig. 6.** Representative XRD patterns of selected samples. (a) Bulk samples and (b) terrigenous components. Cal = calcite; Qtz = quartz; Fs = feldspars; Gt = goethite; Ill = illite; I/S = mixed layers illite/smectite; Chl = chlorite; Kao = kaolinite;  $\Sigma$  Clay minerals = sum clay minerals.

## 5. Discussion

In this section, we first discuss the results of stratigraphic, petrographic and mineralogical analyses to assess the palaeodepositional environments and diagenetic conditions. Then the computed P20, P21 and P10 values are considered, to unravel the fracture stratigraphy properties of the Mesozoic platform carbonates.

### 5.a. Depositional setting

The Apennine Platform is considered as part of the bridge that connected the African Plate to the Adria microplate (Zarcone *et al.* 2010; Randazzo *et al.*, 2021). Its carbonate factory was established during the Late Triassic, and lasted until the middle Cretaceous (Selli, 1957; Sartoni & Crescenti, 1961, 1962).

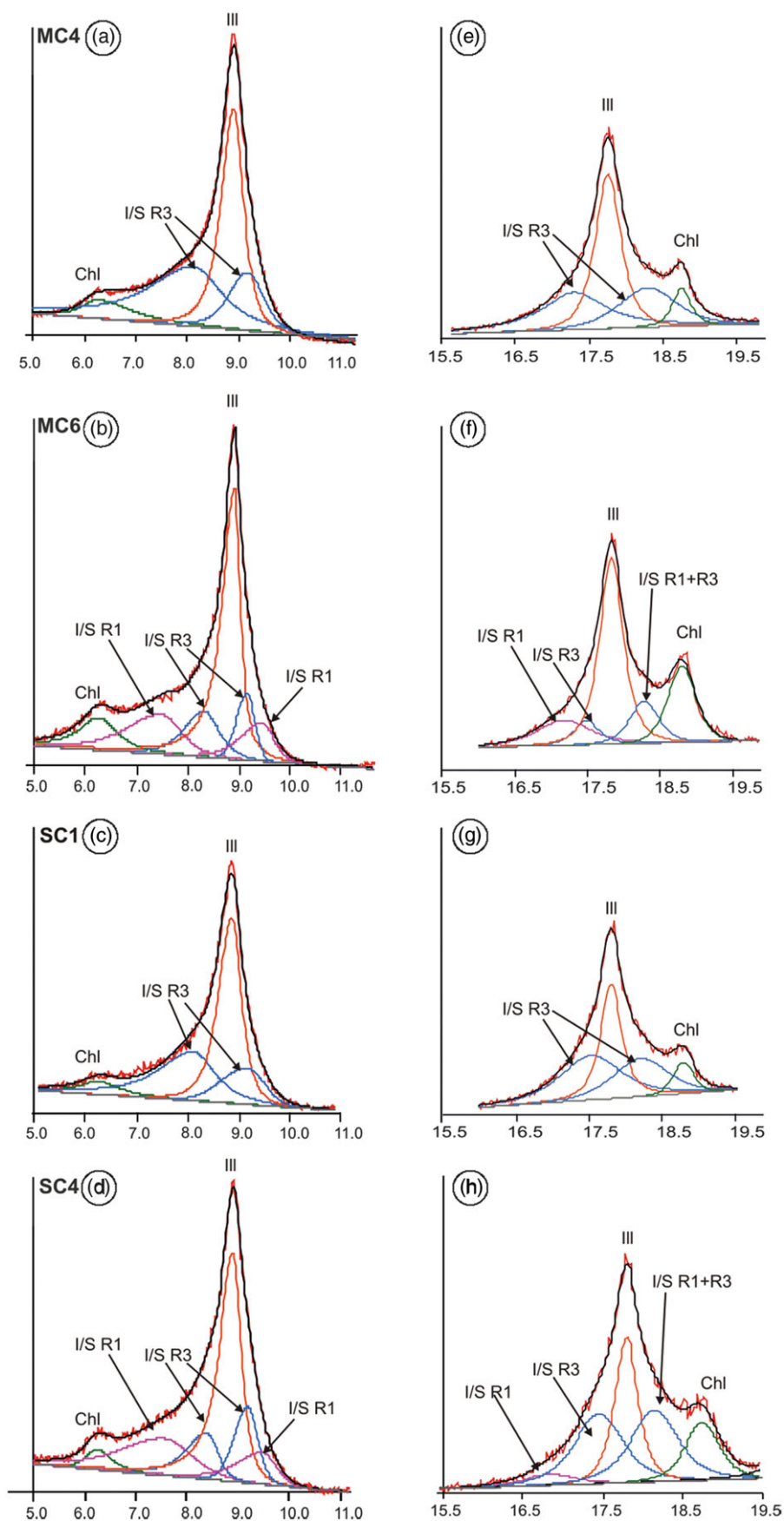


**Fig. 7.** Representative XRD patterns of ethylene glycol solvated clay fraction powders of selected samples. On the left (a–d) decomposition at low angles; on the right (e–h) decomposition at higher angles. III = illite; I/S = mixed layers illite/smectite; Chl = chlorite.



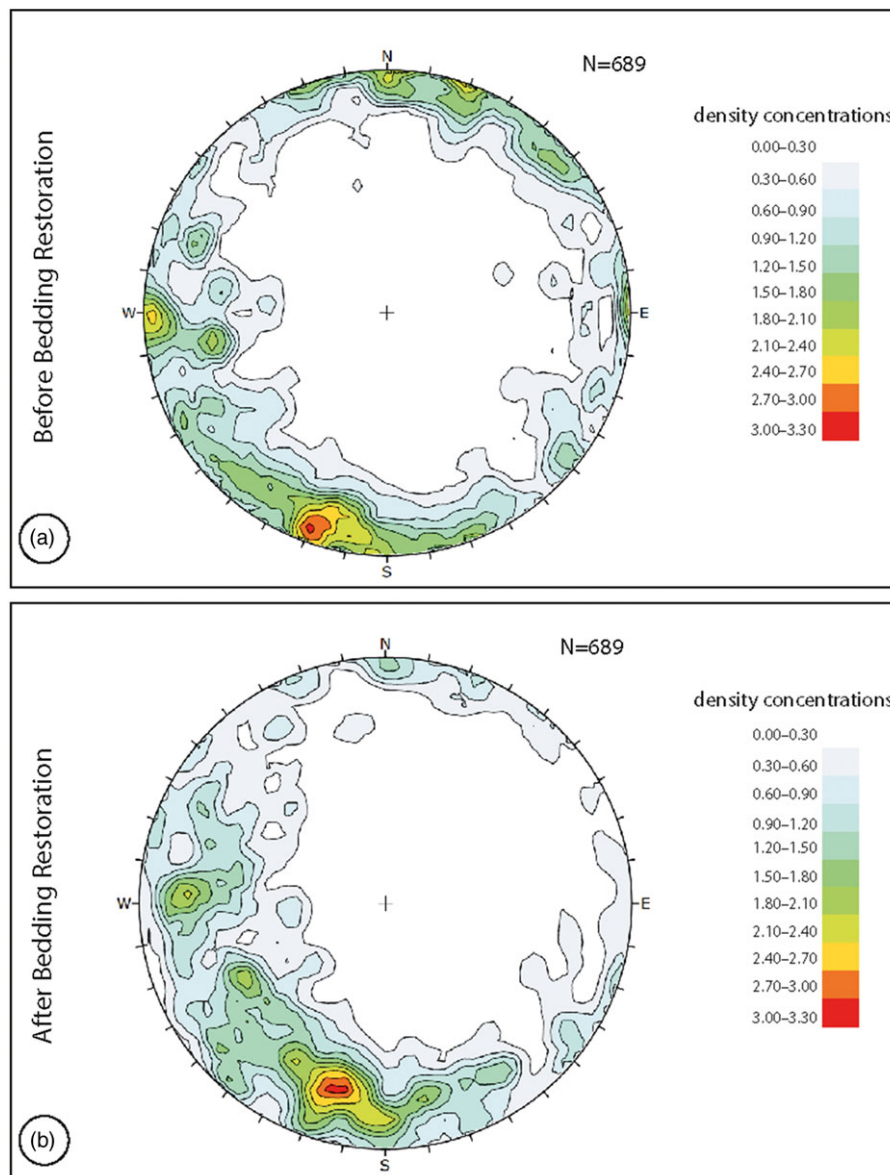


**Fig. 8.** Cumulative lower-hemisphere, equal-area stereographic projection of fracture poles (a) after field measurements and (b) after bedding restoration. Fracture data restored considering the attitude of single beds from which data were gathered.

Previous studies ascribed the Viggiano Mountain carbonates to the Alburno–Cervati Unit (Lechler *et al.* 2012). In this study, we support this interpretation, and provide further constraints for the assessment of their depositional setting.

According to the presence of large benthic foraminifera and algae, the well-layered carbonates formed at tropical and subtropical latitudes within an inner shallow platform environment (Flügel, 2004) characterized by well-oxygenated, warm waters (Fugagnoli, 2004). Furthermore, the presence of ooids, irregular clasts and thick shells of *Lithiotis* bivalves is consistent with occasional turbulent conditions, build-ups and sand shoals (Clari, 1976; Flügel 2004; Gale *et al.* 2005). Accordingly, we assess that carbonate deposition took place in a lagoonal environment protected by sand shoals. The informal litho-biostratigraphic zonation is mainly based on benthic foraminifers and calcareous algae association.

The *Palaeodasycladus mediterraneus* distribution covers the whole Lower Jurassic (Barattolo, 1991); however, the presence of these algae with benthic foraminifera such as *Haurania* sp., *Siphovalvulina* sp. and *Lituosepta* sp. is consistent with upper Sinemurian–Pliensbachian age (Todaro *et al.* 2017 and references therein).

The oolitic carbonates formed in high-energy water conditions, above fair-weather wave base, within depositional environments characterized by a wide, low-gradient ramp rimmed by sand shoals (Flügel, 2004; BouDagher-Fadel, 2008). Formation of the sandy margin was due to the absence of sponge reefs, as a consequence of the end-Triassic mass extinction (Di Stefano *et al.* 1996, Todaro *et al.* 2018). The lithofacies transition between well-layered and oolitic carbonates hence marked both relative deepening and landward migration of the depositional setting, similar to other

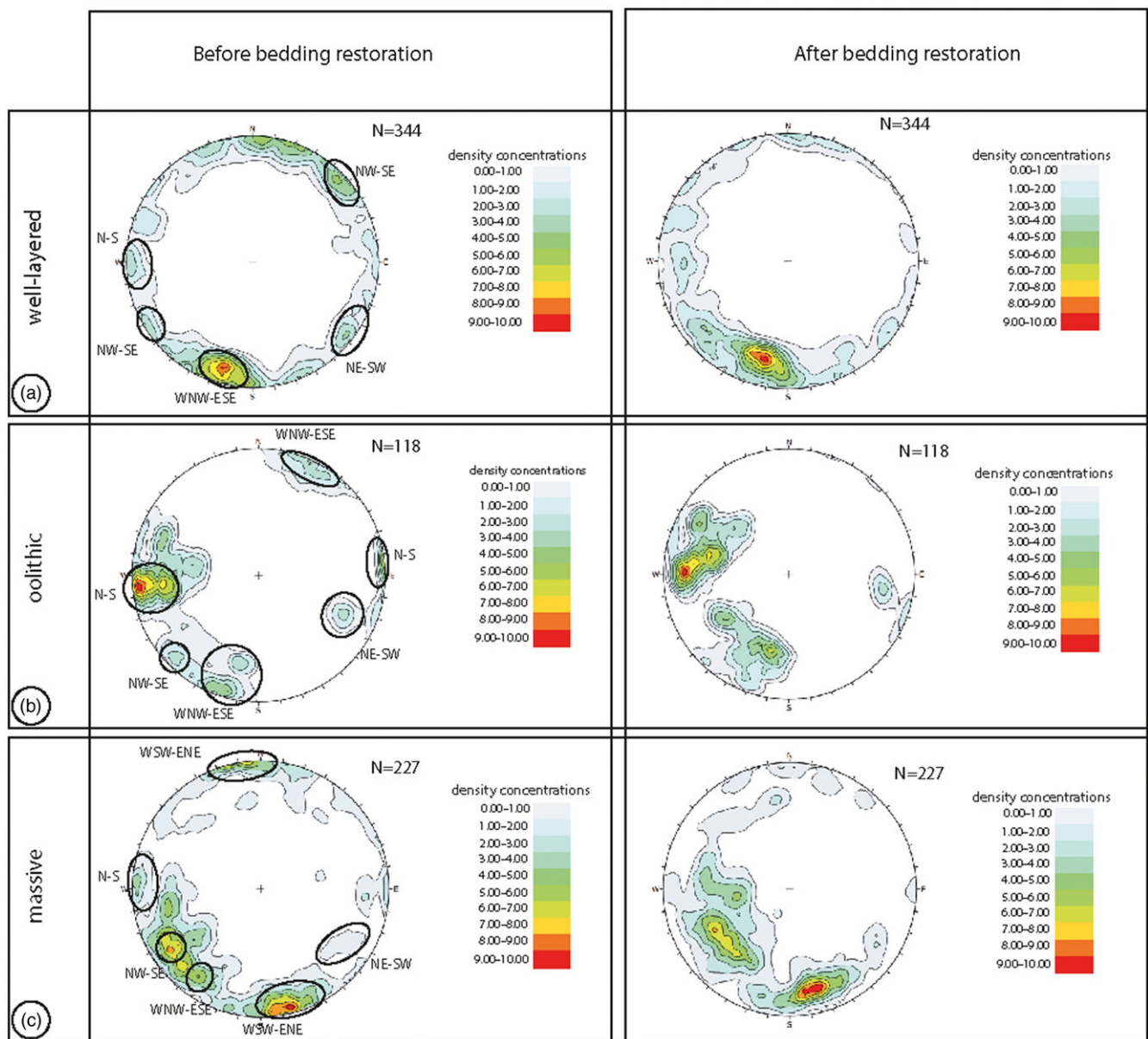


**Fig. 9.** Lower-hemisphere equal-area stereographic projection of fracture poles after field measurements (left) and after bedding restoration (right), subdivided into three subsets, according to the related carbonate units: (a) well-layered carbonates; (b) oolitic carbonates; (c) massive carbonates.

Lower Jurassic carbonate platforms of western Tethys (Mei & Gao, 2012; Ettinger *et al.* 2021). Accordingly, the Pliensbachian–Toarcian extinction is associated with a sequence boundary related to transgression (Hallam, 1997; Haq, 2018), which drowned the carbonate platform and therefore affected the carbonate factory.

The massive carbonates formed in a high-energy shelf environment (Flügel, 2004). In detail, the shallow-water biota, rounded skeletal fragments and/or pristine rudist fossils (*Caprinids* bouquet in growth position; Bentivenga *et al.* 2017) are consistent with moderate- to high-energy depositional environments close to the platform margin (reef to fore-reef) (Di Stefano & Ruberti, 2000; Hughes & Tanner, 2000). On the other hand, the stromatolites, ooids and oncoids are consistent with more internal lagoonal–tidal environments not far from the platform margin, as also documented in northern

Sicily (Di Stefano & Ruberti, 2000). Moreover, the stromatolitic laminae and meniscus cements respectively recorded relative sea level oscillations and near-surface fluid circulation conditions (Flügel, 2004).

### 5.b. Diagenetic evolution

Clay mineral analysis is useful for assessing palaeoclimatic conditions and diagenetic rock evolution (Hoffman & Hower, 1979; Chamley, 1989; Cavalcante *et al.*, 2003, 2011; Mazzoli *et al.*, 2008; Waliczek *et al.*, 2021). The very low amount, or absence, of goethite, kaolinite, hematite and boehmite in the study powders suggests the lack of any terrigenous component associated to possible post-sedimentary reworking processes and/or subaerial alteration (Agosta *et al.* 2021, and references therein). The presence of mixed



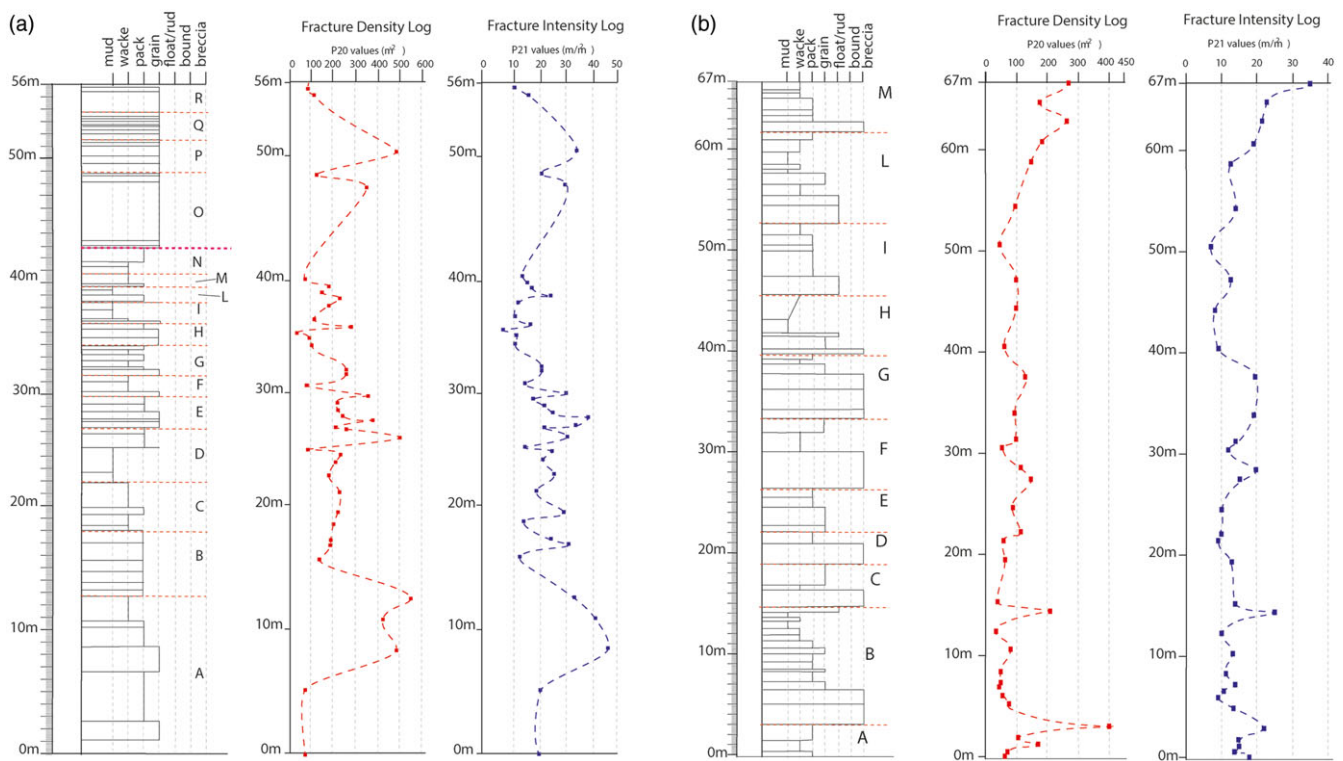


**Fig. 10.** Fracture density (P20) and intensity (P21) logs after field circular scanline measurements conducted across (a) well-layered and oolitic carbonates, and (b) massive carbonates.

illite/smectite layers with R1 and R3 ordering with a high percentage of illite is consistent with *c.* 130 °C thermal maturity, typical of high diagenetic conditions (Merriman & Peacor, 1999; Cavalcante *et al.*, 2012; Perri *et al.*, 2016; Waliczek *et al.*, 2021). However, since smectite illitization and mixed-layer formation are also time-dependent processes (McCubbin & Patton, 1981; Pollastro, 1993), and a function of K-availability (Cavalcante *et al.*, 2007, 2015), we assess 100–130 °C diagenetic temperature range conditions. Assuming 20–25 °C temperature gradients, typical of accretionary wedges (Merriman, 2005), a *c.* 4–5 km burial is therefore estimated for the study carbonates. Considering that the overall platform carbonate thickness is less than 1 km (Patacca & Scandone, 2007), the aforementioned diagenetic conditions were likely related to the structural stacking of the Apennines allochthonous units.

### 5.c. Diffuse vs localized fractures

Within the well-layered carbonates, the exponential fracture spacing distributions assessed for the N292E, N284E and N206E fracture sets are due to a deformation that took place under uniform, remote stress fields (Dershowitz & Einstein, 1988). Fracturing in this case is hence comparable to a Poissonian process (Cruden, 1977), in which the probability that a fracture could enucleate within a given space interval (*i.e.* single carbonate beds) is constant. The three aforementioned fracture sets therefore form a diffuse fracture network, whose failure modes and relative timing of formation are not yet assessed. However, the power-law fracture spacing distributions computed for the N300E, N252E and N180E fracture sets are due to a deformation that occurred under local stress fields (Bonnet *et al.* 2001, and references therein). These fracture sets therefore form a localized network and their fractal

dimension, *D*, corresponds the slope of the best-fit line (Mandelbrot & Wheeler, 1983). The computed *D* values for the three aforementioned localized fracture sets are between 0.56 and 0.76, suggesting poorly developed N180E fractures and moderately developed N300E and N252E fractures, respectively (Gillespie *et al.* 1993). Our results are similar to those gathered by Panza *et al.* (2016) and Giuffrida *et al.* (2019), who respectively documented *D* values between 0.45 and 0.69, and between 0.39 and 0.81 for fractures measured away from major fault zones cross-cutting Apulian platform carbonates. Regarding the Viggiano Mountain study area, Cello *et al.* (2000) also documented a low degree of fracture development within the carbonate fault damage zones, with *D* values between 1.25 and 1.40 after box-counting methodology.

Focusing on the WNW–ESE-striking fractures, the most common set within the well-layered carbonates (*cf.* Fig. 8), both N284E- and N292E-striking fractures pertain to the diffuse network, and the N300E-striking fractures to the localized network. We interpret these results as due to multiple stages of fracture nucleation and subsequent development. Specifically, we propose that the WNW–ESE fractures first nucleated under uniform, remote stress fields likely associated with burial diagenesis (Korneva *et al.* 2014; Lavenu *et al.* 2014; Lavenu & Lamarche, 2018; La Bruna *et al.* 2020; Agosta *et al.* 2021) and/or palaeo-foreland bulging of the carbonates (Tavani *et al.* 2015; Corradetti *et al.* 2018). Subsequently, sub-parallel fractures formed under local stress fields associated with meso-scale faulting, as documented for faulted carbonates of the Apulian Platform exposed in the Majella Mountain (Agosta *et al.* 2010; Volatili *et al.* 2019; Romano *et al.* 2020), and Murge Plateau of Italy (Panza *et al.* 2015, 2016; Zambrano *et al.* 2016).

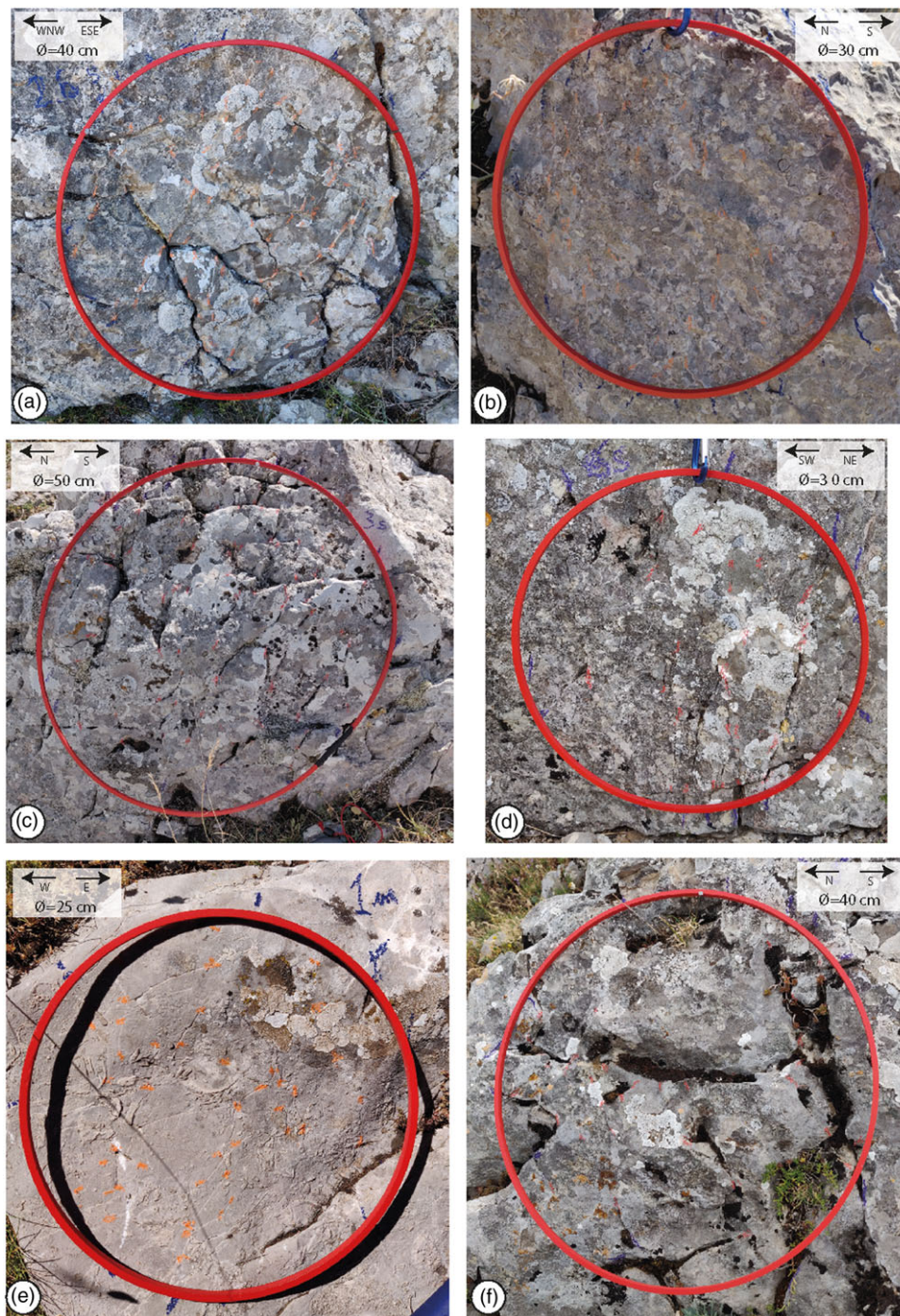


**Fig. 11.** Outcrop images of the investigated carbonate beds by means of circular scanlines: (a, b) well-layered carbonates; (c, d) oolitic carbonates; (e, f) massive carbonates. The right column (a, c, e) shows the beds characterized by high fracture density and intensity; the left column (b, d, f) shows the beds with high fracture density and intensity.

#### 5.d. Fracture stratigraphy

Fracture density is related to nucleating fracture networks according to fracture linkage configuration (Myers & Aydin, 2004; Agosta & Aydin, 2006; De Jossineau & Aydin, 2007; Antonellini *et al.* 2008; Agosta *et al.* 2010), and to rock elastic properties (Gross *et al.* 1995; Agosta *et al.* 2015; Rustichelli *et al.* 2016). However, fracture intensity is associated with well-connected fracture

networks, which often localize within fault damage zones (De Jossineau & Aydin, 2007; Aydin *et al.* 2010; Demurtas *et al.* 2016; Giuffrida *et al.* 2019; Mercuri *et al.* 2020; Camanni *et al.* 2021).

At the Viggiano Mountain, neither P20 nor P21 varies proportionally with the bed thickness (Fig. 14a, d, e). Such a lack of proportionality is also displayed by the P10 values computed for the WNW–ESE (well-layered) and ENE–WSE (massive



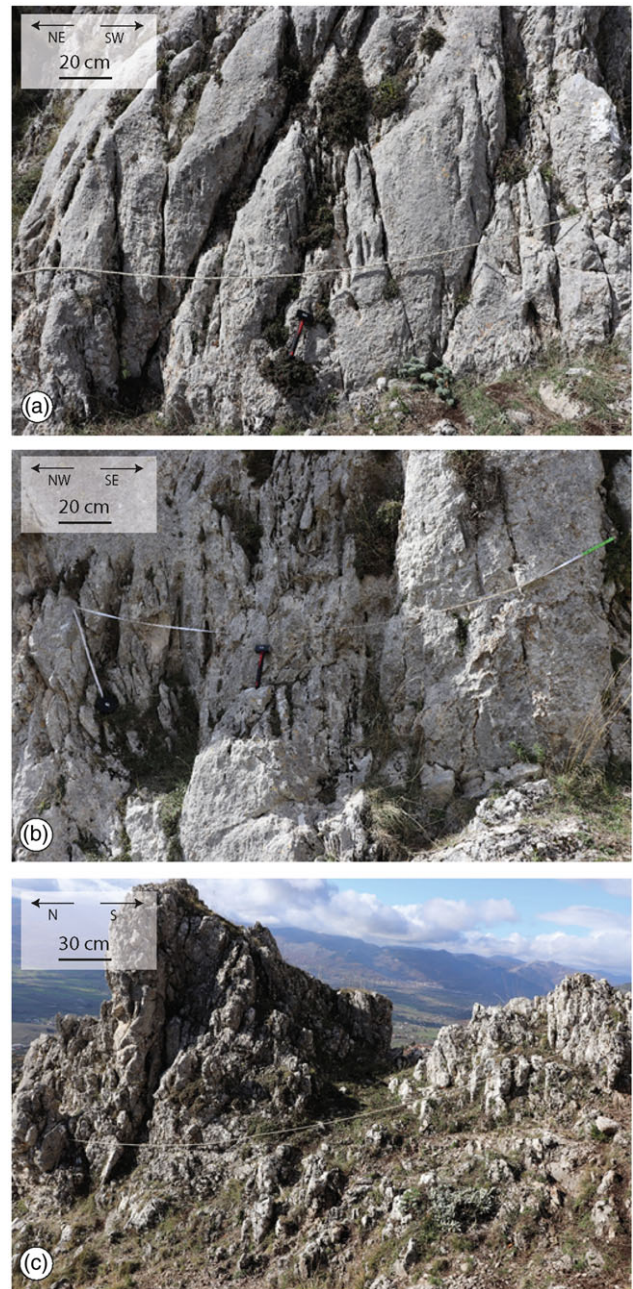
**Table 3.** P10 variations for the JV1 fracture set

Lithofacies	Bed thickness (cm)	P10
Grainstone	60	1.79
Grainstone	70	1.26
Wackestone	25	0.85
Wackestone	54	0.3
Grainstone	25	0.86
Oolitic grainstone	55	1.06
Oolitic grainstone	90	0.74
Carbonate breccia	30	1.35
Carbonate breccia	120	0.95
Carbonate breccia	100	0.46

carbonates)-striking fractures (Fig. 15), the most common in those sedimentary units. This finding contrasts with common spacing distributions documented for single fracture sets in layered rock masses (Nur & Israel, 1980; Gross *et al.* 1995; Bai & Pollard, 2000; Schöpfer *et al.* 2011), and can be explained by the structural complexity of the studied carbonate outcrops, which expose both diffuse and localized fractures (cf. Section 5.c).

The P20 and P21 logs show similar trends in both well-layered and oolitic carbonates (cf. Fig. 10a). In layered carbonates, this is consistent with non-strata-bound fractures forming due to linkage of pre-existing structural elements, and with nucleation of new strata-bound fractures within the narrow process zones that localize at the primary interfaces (Agosta & Aydin, 2006; Antonellini *et al.* 2008; Agosta *et al.* 2009). However, the P20 and P21 values do not show great similarities in the massive carbonates (cf. Fig. 10b). Accordingly, we assess that these carbonates with weak primary interfaces were mainly affected by fracture linkage processes, which dominated over fracture nucleation forming well-developed, vertically persistent fractures. The modalities of fracture propagation across the depositional and diagenetic interfaces exposed at the Scarrone la macchia site are currently under investigation. The results of this work will likely shed light on the deformation mechanisms associated with primary interface disruptions.

Focusing on the possible correlations among P20, P21 and carbonate lithology, we document higher values of both fracture density and intensity in the grain-supported carbonate beds (Fig. 14b, c, f, g). Accordingly, we attribute such a pervasiveness of diffuse fractures to the high values of the elastic moduli that characterized the grain-supported carbonates at times of deformation (*sensu* Bai & Pollard, 2000 and references therein). Our interpretation supports previous data published by Wennberg *et al.* (2006) for carbonates with relatively weak bed interfaces, and by Larsen *et al.* (2010) for rock multilayers in which carbonate mudstone beds arrested/deflected a great number of fractures. We further assess that the relatively high values of the elastic moduli characterized the grain-supported carbonate beds due to burial-related physical/chemical compaction (Rustichelli *et al.* 2012, 2015) and/or cementation processes (Eberli *et al.* 2003; Lamarche *et al.* 2012; Lavenu *et al.* 2014; Lavenu & Lamarche, 2018; La Bruna *et al.* 2020), as suggested by the high P10 values documented in these rocks for the WNW–ESE and WSW–ESE fractures (cf. Table 3).

**Fig. 12.** Outcrop images of the (a) S1, (b) S2 and (c) S3 linear scanlines.

Previous studies have documented the control exerted by carbonate lithofacies on fracture intensity. Mercuri *et al.* (2020) investigated a relay ramp zone in Mesozoic platform carbonates of central Italy, and documented lower P10 in carbonate packstones relative to carbonate grainstones and boundstones. At larger scales of observation, Corradetti *et al.* (2018) documented higher P21 in the dolomitic units encompassed by limestone beds pertaining to Mesozoic platform carbonates exposed in southern Italy. There, diagenetic dolomitization within discrete rock intervals (Vinci *et al.* 2017 and references therein) was invoked as the driving mechanism for fracture localization within specific carbonate beds and bed packages.

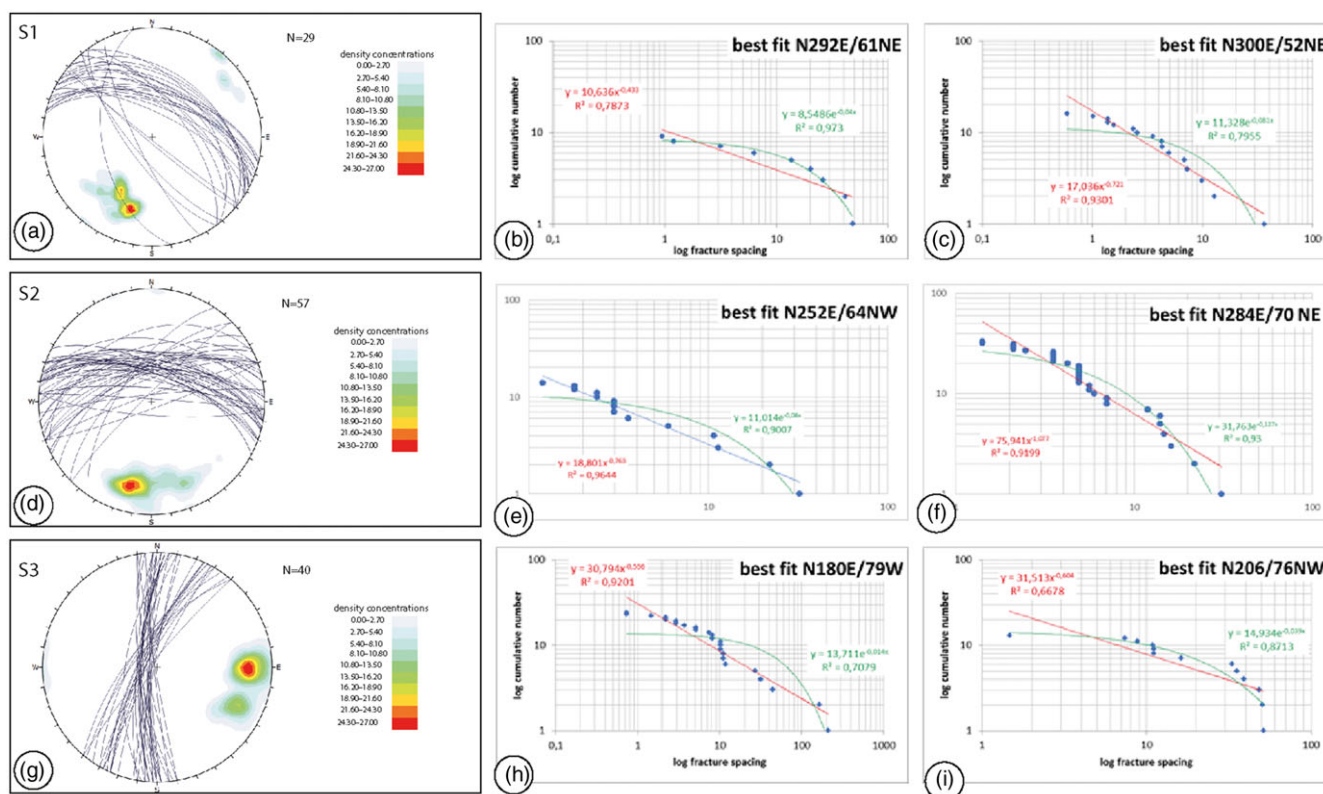


**Fig. 13.** Multiscale fracture spacing distribution. (a) Lower-hemisphere, equal-area stereographic projection of fracture poles of the S1 scanline; (b) log cumulative number vs spacing and best fit relative to the N292 striking set; (c) log cumulative number vs spacing and best fit relative to the N300 striking set; (d) lower-hemisphere, equal-area stereographic projection of fracture poles of the S2 scanline; (e) log cumulative number vs spacing and best fit relative to the N252 striking set; (f) log cumulative number vs spacing and best fit relative to the N284 striking set; (g) lower-hemisphere, equal-area stereographic projection of fracture poles of the S3 scanline; (h) log cumulative number vs spacing and best fit relative to the N180 striking set; (i) log cumulative number vs spacing and best fit relative to the N206 striking set.

## 6. Conclusions

This work focused on the palaeodepositional settings, amount of overburden and fracture stratigraphy of Mesozoic platform carbonates exposed at the Viggiano Mountain area, southern Italy. In particular, three main depositional units, respectively labelled as well-layered, oolitic and massive carbonates, were investigated. The Sinemurian–Pleinsbachian well-layered carbonates formed in a lagoonal environment protected by sand shoals. They include both mm-thick bed interfaces with pressure solution seams and cm-thick bed package interfaces including small amounts of terrigenous material. The Toarcian oolitic carbonates were deposited in a ramp rimmed by sand shoals. The oolitic carbonates contain amalgamated carbonate beds, and bed package interfaces made up of mm-thick terrigenous laminae. A large-scale stratigraphic interface including 10–15 cm thick mixed carbonate–terrigenous rock was documented between the two aforementioned sedimentary units. However, the Cenomanian massive carbonates were deposited in a moderate- to high-energy setting, not far from the platform margin. These rocks are primarily made up of primary breccia and rudist fragments. The well-layered carbonates were subjected to a thermal temperature of 100–130 °C, as shown by the R1 and R3 ordering of illite/smectite documented after XRPD analyses of carbonate powders. Such a temperature was associated with 4–5 km of burial depth associated with the structural stacking of the allochthonous units of the southern Apennines fold-and-thrust belt.

Results of quantitative field structural analysis were consistent with the presence of five main sets of high-angle fractures. According to the results of linear scanline measurements, both diffuse and localized fracture networks cross-cut the study carbonates. The former network includes two orthogonal, high-angle fracture sets striking *c.* ENE–WSW and SSW–NNE. However, the localized network is made up of ENE–WSW-, ESE–WNW- and N–S-striking high-angle fractures. According to the computed *D* values, the localized fracture sets were interpreted as characterized by a low degree of maturity. Results of circular scanline measurements showed similar trends of both P20 and P21 throughout the well-layered and oolitic carbonate successions. Such similarity was interpreted as due to fault-related fracturing, which mainly localized across primary heterogeneities such as bed and bed-package interfaces. The vertical growth of incipient slip surfaces by linkage of pre-existing structural elements was affected by the mechanical control exerted by the aforementioned interfaces. However, P20 and P21 do not show very similar trends throughout the massive carbonates due to pronounced bed amalgamation.

Results of fracture stratigraphy analysis hence showed that the computed P20 and P21 did not vary in proportion to bed thickness. These results contrasted with common spacing distributions documented for single fracture sets in layered rock masses, and were interpreted in light of the structural complexity of the studied carbonate outcrops exposing both diffuse and localized fractures. On



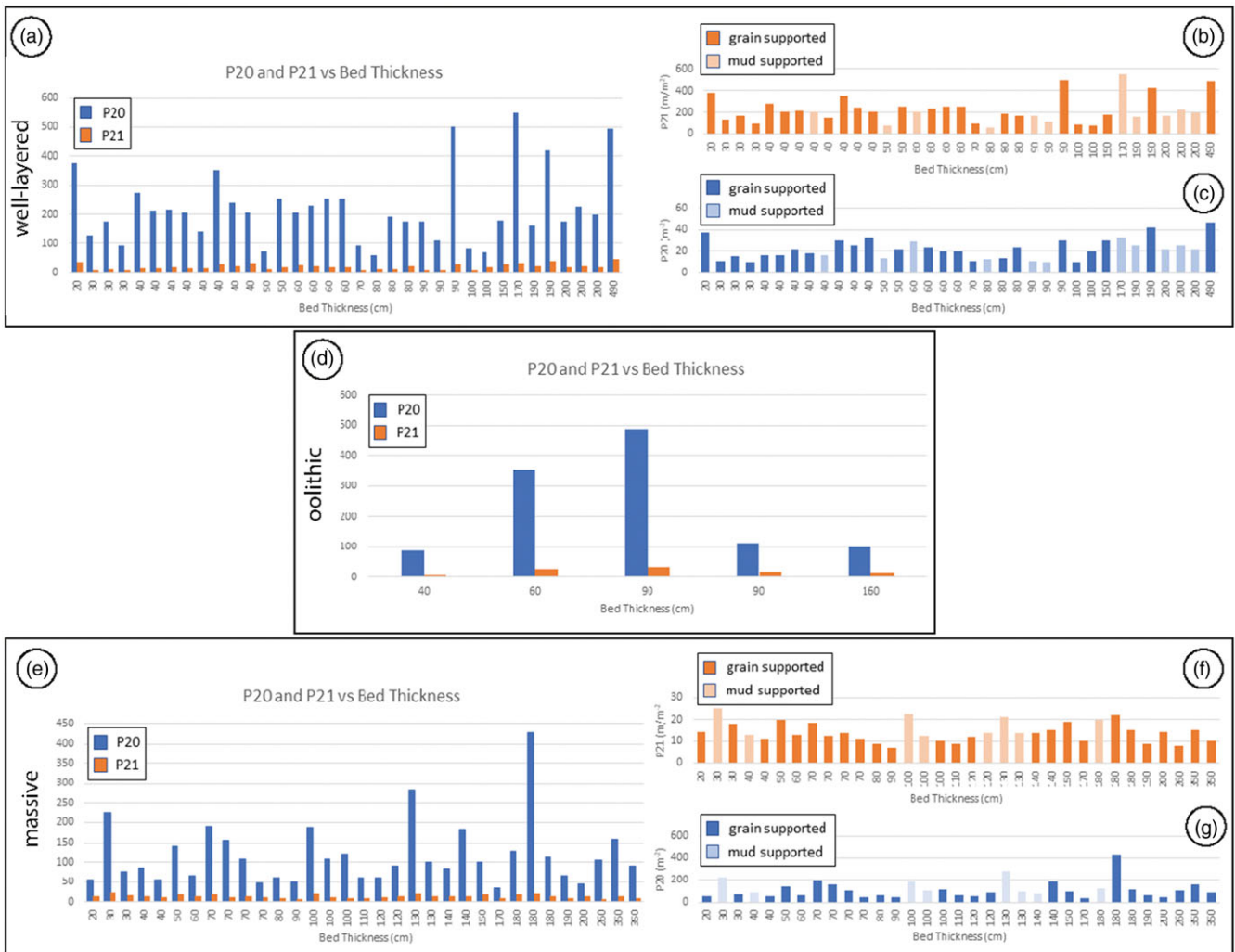


**Fig. 14.** (a, d, e) Bed thickness vs P20 and P21 values for (a) well-layered carbonates; (d) oolitic carbonates; (e) massive carbonates. (b) Bed thickness vs P20 for the mud-supported carbonate, in which the grain-supported and the mud-supported beds are highlighted; (c) bed thickness vs P21 for the mud-supported carbonate, in which the grain-supported and the mud-supported beds are highlighted; (f) bed thickness vs P20 for the massive carbonate, in which the grain-supported and the mud-supported beds are highlighted; (g) bed thickness vs P21 for the massive carbonate, in which the grain-supported and the mud-supported beds are highlighted.

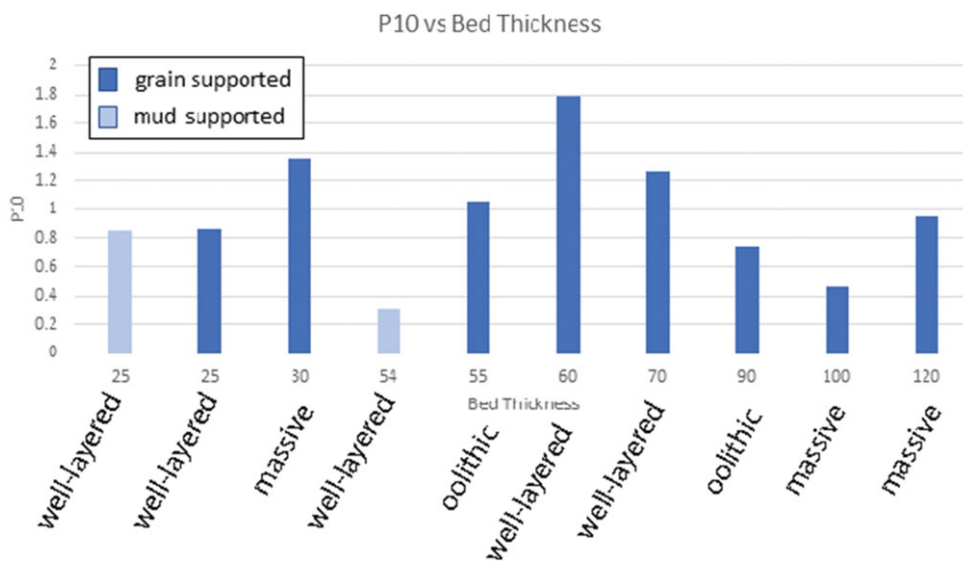


**Fig. 15.** Bed thickness vs P10 values calculated through significant beds in the three carbonate units. The grain-supported lithofacies and the mud-supported lithofacies are highlighted.

the other hand, similar to P10 computed for the most common diffuse fracture sets, both P20 and P21 showed the highest values in correspondence to the coarse-grained carbonate beds. These data are explained by taking into account the burial-related physical–chemical compaction and/or cementation processes. They profoundly affect the mechanical properties of the carbonate multilayers, determining fracture pervasiveness within carbonate beds with the original larger pore space. Further analyses will be required to assess the specific diagenetic mechanisms associated with overburden, which likely played a major role in the fracture stratigraphy of the studied Mesozoic carbonates.

**Acknowledgements.** This work is part of the first author's PhD research work. C.M. acknowledges the help and contribution provided by Grazia de Grazia, Innocenzo Manniello and Giulia Schirripa Spagnolo during fieldwork. Previous work by Nicola Costantino is acknowledged. The revisions of Andrea Billi and of two anonymous referees, as well as comments provided by the guest editor Stefano Tavani, greatly improved the quality of this work. This research is supported by the Reservoir Characterization Project ([www.rechproject.com](http://www.rechproject.com)) and by Eni SpA.

**Conflict of interest.** The authors declare that there is no conflict of interest.

## References

- Agosta F, Alessandrini M, Antonellini M, Tondi E and Giorgioni M (2010) From fractures to flow: a field-based quantitative analysis of an outcropping carbonate reservoir. *Tectonophysics* **490**, 197–213.
- Agosta F, Alessandrini M, Tondi E and Aydin A (2009) Oblique normal faulting along the northern edge of the Majella Anticline, central Italy: inferences on hydrocarbon migration and accumulation. *Journal of Structural Geology* **31**, 1317–33.
- Agosta F and Aydin A (2006) Architecture and deformation mechanism of a basin-bounding normal fault in Mesozoic platform carbonates, central Italy. *Journal of Structural Geology* **28**, 1445–67.
- Agosta F, Manniello C, Cavalcante F, Belviso C and Prosser G (2021) Late Cretaceous transtensional faulting of the Apulian Platform, Italy. *Marine and Petroleum Geology* **127**, 104889.
- Agosta F, Wilson C and Aydin A (2015) The role of mechanical stratigraphy on normal fault growth across a Cretaceous carbonate multi-layer, central Texas (USA). *Italian Journal of Geosciences* **134**, 423–41.
- Allmendinger RW, Cardozo N and Fisher DM (2011) *Structural Geology Algorithms: Vectors and Tensors*. Cambridge: Cambridge University Press.
- Amodio-Morelli L, Bonardi G, Colonna V, Dietrich D, GiunTa G, Ippolito F, Liguori V, Lorenzoni S, Paglionico A, Perrone V, Piccarreta G, Russo M, Scandone P, Zanettin-Lorenzoni E and Zuppetta A (1976) L'Arco calabro-peloritano nell'orogene appenninico-maghrebide. *Memorie della Società Geologica Italiana* **17**, 1–60.
- Andreo B, Vías J, Durán JJ, Jiménez P, López-Geta JA and Carrasco F (2008) Methodology for groundwater recharge assessment in carbonate aquifers: application to pilot sites in southern Spain. *Hydrogeology Journal* **16**, 911–25.
- Antonellini M, Tondi E, Agosta F, Aydin A and Cello G (2008) Failure modes in deep-water carbonates and their impact for fault development: Majella Mountain, Central Apennines, Italy. *Marine and Petroleum Geology* **25**, 1074–96.
- Aydin A, Antonellini M, Tondi E and Agosta F (2010) Deformation along the leading edge of the Maiella thrust sheet in central Italy. *Journal of Structural Geology* **32**, 1291–304.
- Bai T and Pollard DD (2000) Fracture spacing in layered rocks: a new explanation based on the stress transition. *Journal of Structural Geology* **22**, 43–57.
- Barattolo F (1991) Mesozoic and Cenozoic marine benthic calcareous algae with particular regard to Mesozoic Dasycladaleans. In *Calcareous Algae and Stromatolites* (ed. R Riding), Berlin, Heidelberg: Springer, pp. 504–40.
- Barattolo F and Romano R (2005) Shallow carbonate platform bioevents during the Upper Triassic–lower Jurassic: an evolutive interpretation. *Bollettino della Società Geologica Italiana* **124**, 123–42.
- Becker A and Gross MR (1996) Mechanism for joint saturation in mechanically layered rocks: an example from southern Israel. *Tectonophysics* **257**, 223–37.
- Bellani S, Brogi A, Lazzarotto A, Liotta D and Ranalli G (2004) Heat flow, deep temperatures and extensional structures in the Larderello Geothermal Field (Italy): constraints on geothermal fluid flow. *Journal of Volcanology and Geothermal Research* **132**, 15–29.
- Bentivenga M, Palladino G, Prosser G, Guglielmi P, Geremia F and Laviano A (2017) A geological itinerary through the Southern Apennine Thrust Belt (Basilicata – Southern Italy). *Geoheritage* **9**, 1–17.
- Berry MD, Stearns DW, Friedman M (1996) The development of a fractured reservoir model for the palm valley gas field. *The APPEA Journal* **36**(1), 82.
- Bonnet E, Bour O, Odling NE, Davy P, Main I, Cowie P and Berkowitz B (2001) Scaling of fracture systems in geological media. *Reviews of Geophysics* **39**, 347–83.
- BouDagher-Fadel MK (2008) The Cenozoic larger benthic foraminifera: the Palaeogene. In *Developments in Palaeontology and Stratigraphy* (ed. MK BouDagher-Fadel), Amsterdam: Elsevier, 21, pp. 297–418, 545.
- Bruno MC, Caliri A, Carbone S, Chiochini M, Di Stefano A, Giano SI, Guarnieri P, Lentini F, Martorano S and Piccarreta G (2014) Carta Geologica d'Italia, Foglio 505 Moliterno, scala 1: 50.000. ISPRA, Servizio Geologico d'Italia. Available online: [https://www.isprambiente.gov.it/Media/carg/505\\_MOLITERNO/Foglio.html](https://www.isprambiente.gov.it/Media/carg/505_MOLITERNO/Foglio.html) (Accessed on 28 October 2021).
- Buttinelli M, Improta L, Bagn S and Chiarabba C (2016) Inversion of inherited thrusts by wastewater injection induced seismicity at the Val d'Agri oil-field (Italy). *Scientific Reports* **6**, 1–8.
- Camanni G, Vinci F, Tavani S, Ferrandino V, Mazzoli S, Corradetti A, Parente M and Iannace A (2021) Fracture density variations within a reservoir-scale normal fault zone: a case study from shallow-water carbonates of southern Italy. *Journal of Structural Geology* **151**, 104432.
- Caruthers AH, Smith PL, Gröcke DR (2013) The Pliensbachian-Toarcian (Early Jurassic) extinction, a global multi-phased event. *Palaeogeography, Palaeoclimatology, Palaeoecology* **386**(2013), 104–18.
- Casero P, Roure F, Endignoux L, Moretti I, Müller C, Sage L and Vially R (1988) Neogene geodynamic evolution of the Southern Apennines. *Memorie della Società Geologica Italiana*, **41**, 109–20.
- Casero P, Roure F and Vially R (1991) Tectonic framework and petroleum potential of the southern Apennines. In *Generation, Accumulation, and Production of Europe's Hydrocarbons* (ed AM Spencer), pp. 381–7. European Association of Petroleum Geoscientists, Special Publication no. 1.
- Cavalcante F, Belviso C, Bentivenga M, Fiore S and Prosser G (2011) Occurrence of palygorskite and sepiolite in upper Paleocene – middle Eocene marine deep sediments of the Lagonegro basin (Southern Apennines – Italy): paleoenvironmental and provenance inferences. *Sedimentary Geology*, **233**, 42–52.
- Cavalcante F, Belviso C, Laurita S and Prosser G (2012) P-T constraints from phyllosilicates of the Liguride Complex of the Pollino area (Southern Apennines, Italy): geological inferences. *Ofioliti* **37**, 65–75.
- Cavalcante F, Fiore S, Lettino A, Piccarreta G and Tateo F (2007) Illite-smectite mixed layers in Sicilide shales and piggy-back deposits of the Gorgoglione Formation (southern Apennines): geological inference. *Bollettino della Società Geologica Italiana* **126**, 241–54.
- Cavalcante F, Fiore S, Piccarreta G and Tateo F (2003) Geochemical and mineralogical approaches to assessing provenance and deposition of shales: a case study. *Clay Minerals* **38**, 383–97.
- Cavalcante F, Prosser G, Agosta F, Belviso C and Corrado G (2015) Post-depositional history of the Miocene Gorgoglione Formation (Southern Apennines, Italy): inferences from mineralogical and structural analyses. *Bulletin de la Société Géologique de France* **186**(4–5), 243–56.
- Cello G, Gambini R, Mazzoli S, Read A, Tondi E and Zucconi V (2000) Fault zone characteristics and scaling properties of the Val d'Agri Fault system (southern Apennines, Italy). *Journal of Geodynamics* **29**, 293–307.
- Cello G and Mazzoli S (1998) Apennine tectonics in southern Italy: a review. *Journal of Geodynamics* **27**, 191–211.
- Cello G, Tondi E, Micarelli L and Mattioni L (2003) Active tectonics and earthquake sources in the epicentral area of the 1857 Basilicata earthquake (southern Italy). *Journal of Geodynamics* **36**, 37–50.
- Chamley H (1989) *Clay Sedimentology*. Berlin and Heidelberg: Springer-Verlag, 623 pp.

- Chiocchini M, Farinacci A, Mancinelli A, Molinari V and Potetti M** (1994) Biostratigrafia a foraminiferi, dasciudadali e calpionelle delle successioni carbonatiche mesozoiche dell'Appennino centrale (Italia). In *Biostratigrafia dell'Italia centrale* (ed A Mancinelli), pp. 9–129. Studi Geologici Camerti, Volume Speciale.
- Clari P** (1976) Caratteristiche sedimentologiche e paleontologiche di alcune sezioni dei Calcarei Grigi del Veneto. *Memorie della Società Geologica Italiana, Padova* **31**, 1–63.
- Corniello A, Ducci D, Ruggieri G and Iorio M** (2018) Complex groundwater flow circulation in a carbonate aquifer: Mount Massico (Campania Region, Southern Italy). Synergistic hydrogeological understanding. *Journal of Geochemical Exploration* **190**, 253–64.
- Corradetti A, Tavani S, Parente M, Iannace A, Vinci F, Pirmez C, Torrieri S, Giorgioni M, Pignalosa A and Mazzoli S** (2018) Distribution and arrest of vertical through-going joints in a seismic-scale carbonate platform exposure (Sorrento peninsula, Italy): insights from integrating field survey and digital outcrop model. *Journal of Structural Geology* **108**, 121–36.
- Cruden DM** (1977) Describing the size of discontinuities. *International Journal of Rock Mechanics and Mining Sciences and Geomechanics Abstracts* **14**, 133–7.
- Cuadros J and Altaner SP** (1998) Characterization of mixed-layer illite-smectite from bentonites using microscopic, chemical, and X-ray methods: constraints on the smectite-to-illite transformation mechanism. *American Mineralogist* **83**, 762–74.
- De Castro P** (1991) Mesozoic. In *5th International Symposium on Fossil Algae. Field Trip Guide-Book* (eds F Barattolo, P De Castro and M Parente), pp. 21–38. Naples: Giannini.
- De Jousseineau G and Aydin A** (2007) The evolution of the damage zone with fault growth in sandstone and its multiscale characteristics. *Journal Of Geophysical Research: Solid Earth* **112**, B12401.
- Demurtas M, Fondriest M, Balsamo F, Clemenzi L, Storti F, Bistacchi A and Di Toro G** (2016) Structure of a normal seismogenic fault zone in carbonates: the Vado di Corno Fault, Campo Imperatore, Central Apennines (Italy). *Journal of Structural Geology* **90**, 185–206.
- Dershowitz WS and HH Einstein** (1988) Characterizing rock joint geometry with joint system models. *Rock Mechanics and Rock Engineering* **21**, 21–51.
- Dershowitz WS and Herda HH** (1992) Interpretation of fracture spacing and intensity. In *The 33rd US Symposium on Rock Mechanics (USRMS)*, ARMA-92-0757.
- Di Niro A, Giano SI and Santangelo N** (1992) Primi dati sull'evoluzione geomorfologica e sedimentaria del bacino dell'alta val d'Agri (Basilicata). *Studi Geologici Camerti* **1**, 257–63.
- Di Stefano P, Alessi A and Gullo M** (1996) Mesozoic and Paleogene megabreccias in southern Sicily: new data on the Triassic paleomargin of the Siculo-Tunisian platform. *Facies* **34**, 101–22.
- Di Stefano P and Ruberti D** (2000) Cenomanian rudist-dominated shelf-margin limestones from the Panormide carbonate platform (Sicily, Italy): facies analysis and sequence stratigraphy. *Facies* **42**, 133–60.
- Dogliani C, Harabaglia P, Martinelli G, Mongelli F and Zito G** (1996) A geodynamic model of the Southern Apennines accretionary prism. *Terra Nova* **8**, 540–7.
- Dunham RJ** (1962) Classification of carbonate rocks according to depositional texture. In *Classification of Carbonate Rocks – A Symposium* (ed. WE Ham), Tulsa, OK: American Association of Petroleum Geologists, pp. 108–21.
- Eberli GP, Baechle GT, Anselmetti FS and Incze ML** (2003) Factors controlling elastic properties in carbonate sediments and rocks. *Leading Edge (Tulsa, OK)* **22**, 654–60.
- Embry AF and Klovan JE** (1971) A Late Devonian reef tract on northeastern Banks Island, N.W.T. *Bulletin of Canadian Petroleum Geology* **19**, 730–81.
- Ettinger NP, Larson TE, Kerans C, Thibodeau AM, Hattori KE, Kacur SM and Martindale RC** (2021) Ocean acidification and photic-zone anoxia at the Toarcian Oceanic Anoxic Event: insights from the Adriatic carbonate platform. *Sedimentology* **68**, 63–107.
- Flügel E** (2004) Carbonate depositional environments. In *Microfacies of Carbonate Rocks* (ed. E Flügel), Berlin, Heidelberg: Springer, pp. 7–52.
- Fugagnoli A** (2004) Trophic regimes of benthic foraminiferal assemblages in Lower Jurassic shallow water carbonates from northeastern Italy (Calcarei Grigi, Trento Platform, Venetian Prealps). *Palaeogeography, Palaeoclimatology, Palaeoecology* **205**, 111–30.
- Gale AS, Kennedy WJ, Voigt S and Walaszczyk I** (2005) Stratigraphy of the Upper Cenomanian-Lower Turonian Chalk succession at Eastbourne, Sussex, UK: ammonites, inoceramid bivalves and stable carbon isotopes. *Cretaceous Research* **26**, 460–87.
- Giano SI, Maschio L, Alessio M, Ferranti L, Improta S and Schiattarella M** (2000) Radiocarbon dating of active faulting in the Agri high. *Journal of Geodynamics* **29**, 371–86.
- Gillespie PA, Howard CB, Walsh JJ and Watterson J** (1993) Measurement and characterisation of spatial distributions of fractures. *Tectonophysics* **226**, 113–41.
- Giuffrida A, Agosta F, Rustichelli A, Panza E, La Bruna V, Eriksson M, Torrieri S and Giorgioni M** (2020) Fracture stratigraphy and DFN modelling of tight carbonates, the case study of the Lower Cretaceous carbonates exposed at the Monte Alpi (Basilicata, Italy). *Marine and Petroleum Geology* **112**, 104045.
- Giuffrida A, La Bruna V, Castelluccio P, Panza E, Rustichelli A, Tondi E, Giorgioni M and Agosta F** (2019) Fracture simulation parameters of fractured reservoirs: analogy with outcropping carbonates of the Inner Apulian Platform, southern Italy. *Journal of Structural Geology* **123**, 18–41.
- Gross MR** (1993) The origin and spacing of cross joints: examples from the Monterey Formation, Santa Barbara Coastline, California. *Journal of Structural Geology* **15**, 737–51.
- Gross MR, Fischer MP, Engelder T and Greenfield RJ** (1995) Factors controlling joint spacing in interbedded sedimentary rocks: integrating numerical models with field observations from the Monterey Formation, USA. *Geological Society, London, Special Publication* **92**, 215–33.
- Gross MR, Gutiérrez-Alonso G, Bai T, Wacker MA, Collinsworth KB and Behl RJ** (1997) Influence of mechanical stratigraphy and kinematics on fault scaling relations. *Journal of Structural Geology* **19**, 171–83.
- Hager BH, Dieterich J, Frohlich C, Juanes R, Mantica S, Shaw JH, Bottazzi F, Caresani F, Castineira D, Cominelli A, Meda M, Osculati L, Petroselli S and Plesch A** (2021) A process-based approach to understanding and managing triggered seismicity. *Nature* **595**, 684–9.
- Hallam A** (1997) Estimates of the amount and rate of sea-level change across the Rhaetian—Hettangian and Pliensbachian—Toarcian boundaries (latest Triassic to early Jurassic). *Journal of the Geological Society* **154**(5), 773–79.
- Haq BU** (2018) Jurassic sea-level variations: a reappraisal. *GSA Today* **28**(1), 4–10.
- Hippolyte JC, Angelier J and Barrier E** (1995) Compressional and extensional tectonics in an arc system: example of the Southern Apennines. *Journal of Structural Geology* **17**, 1725–40.
- Hoffman J and Hower J** (1979) Clay mineral assemblages as low grade metamorphic geothermometers: application to the thrust faulted disturbed belt of Montana. In *Aspects of Diagenesis* (eds PA Scholle and PS Schluger), pp. 55–79. SEPM, Special Publication no. 26.
- Hughes TP and Tanner JE** (2000) Recruitment failure, life histories, and long-term decline of Caribbean corals. *Ecology* **81**, 2250.
- Improta L, Iannaccone G, Capuano P, Zollo A and Scandone P** (2000) Inferences on the upper crustal structure of Southern Apennines (Italy) from seismic refraction investigations and subsurface data. *Tectonophysics* **317**, 273–97.
- Kastens K and Mascle J** (1990) The geological evolution of the Tyrrhenian Sea: an introduction to the scientific results of ODP Leg 107. *Proceedings of the Ocean Drilling Program, Scientific Results, Leg 107, Tyrrhenian Sea*, pp. 3–26. College Station, Texas.
- Korneva I, Tondi E, Agosta F, Rustichelli A, Spina V, Bitonte R and Di Cuia R** (2014) Structural properties of fractured and faulted Cretaceous platform carbonates, Murge Plateau (southern Italy). *Marine and Petroleum Geology* **57**, 312–26.
- La Bruna V, Lamarche J, Agosta F, Rustichelli A, Giuffrida A, Salardon R and Marié L** (2020) Structural diagenesis of shallow platform carbonates: role of early embrittlement on fracture setting and distribution, case study of Monte Alpi (Southern Apennines, Italy). *Journal of Structural Geology* **131**, 103940.
- Lamarche J, Lavenu APC, Gauthier BDM, Guglielmi Y and Jayet O** (2012) Relationships between fracture patterns, geodynamics and mechanical stratigraphy in Carbonates (South-East Basin, France). *Tectonophysics* **581**, 231–45.



- Larsen B, Gudmundsson A, Grunnaleite I, Sælen G, Talbot MR and Buckley SJ (2010) Effects of sedimentary interfaces on fracture pattern, linkage, and cluster formation in peritidal carbonate rocks. *Marine and Petroleum Geology* 27, 1531–50.
- Laubach SE, Olson JE and Cross MR (2009) Mechanical and fracture stratigraphy. *AAPG Bulletin* 93, 1413–26.
- Lavenu APC and Lamarche J (2018) What controls diffuse fractures in platform carbonates? Insights from Provence (France) and Apulia (Italy). *Journal of Structural Geology* 108, 94–107.
- Lavenu APC, Lamarche J, Salardon R, Gallois A, Marié L and Gauthier BDM (2014) Relating background fractures to diagenesis and rock physical properties in a platform-slope transect. Example of the Maiella Mountain (central Italy). *Marine and Petroleum Geology* 51, 2–19.
- Lechler M, G Frijia, M Mutti, G Palladino and G Prosser (2012) Stratigraphic setting of a segment from the Eastern margin of the Apennine platform (Monte di Viggiano, Southern Apennines). *Rendiconti Online S.G.I.* 21, 1012–3.
- Lucia FJ (1983) Petrophysical parameters estimated from visual descriptions of carbonate rocks: a field classification of carbonate pore space. *JPT, Journal of Petroleum Technology* 35, 629–37.
- Lucia FJ and Fogg GE (1990) Geologic/stochastic mapping of heterogeneity in a carbonate reservoir. *JPT, Journal of Petroleum Technology* 42, 1298–303.
- Malinverno A and Ryan WBF (1986) Extension in the Tyrrhenian Sea and shortening in the Apennines as result of arc migration driven by sinking of the lithosphere. *Tectonics* 5, 227–45.
- Mallet R (1862) *Great Neapolitan Earthquake of 1857: The First Principles of Observational Seismology, 2 vols.* London: Chapman and Hall, pp. 486–94.
- Mandelbrot BB and Wheeler JA (1983) The fractal geometry of nature. *American Journal of Physics* 51, 286–7.
- Marín AI and Andreo B (2015) Vulnerability to contamination of karst aquifers. In *Karst Aquifers—Characterization and Engineering* (ed. Z Stevanović), Professional Practice in Earth Sciences. Cham: Springer, pp. 251–66.
- Maschio L, Ferranti L and Burrato P (2005) Active extension in Val d'Agri area, southern Apennines, Italy: implications for the geometry of the seismogenic belt. *Geophysical Journal International* 162, 591–609.
- Mauldon M, Dunne WM and Rohrbach MB (2001) Circular scanlines and circular windows: new tools for characterizing the geometry of fracture traces. *Journal of Structural Geology* 23, 247–58.
- Mazzoli S, D'Errico M, Aldega L, Corrado S, Invernizzi C, Shiner P and Zattin M (2008) Tectonic burial and “young” (<10 Ma) exhumation in the southern Apennines fold-and-thrust belt (Italy). *Geology* 36, 243–6.
- McCubbin DG and Patton JW (1981) Burial diagenesis of illite/smectite: the kinetic model. *American Association of Petroleum Geologists Bulletin* 65, 956.
- Mei M and Gao J (2012) Giant Induan oolite: a case study from the Lower Triassic Daye Formation in the western Hubei Province, South China. *Geoscience Frontiers* 3, 843–51.
- Mercuri M, Carminati E, Tartarello MC, Brandano M, Mazzanti P, Brunetti A, McCaffrey KJW and Collettini C (2020) Lithological and structural control on fracture frequency distribution within a carbonate-hosted relay ramp. *Journal of Structural Geology* 137, 104085.
- Merriman RJ and Peacor DR (1999) Very low-grade metapelites; mineralogy, microtextures and measuring reaction progress. In *Low-Grade Metamorphism* (eds M Frey and D Robinson), Oxford, UK: Blackwell Science, pp. 10–60.
- Merriman RJ (2005) Clay minerals and sedimentary basin history. *European Journal of Mineralogy* 17, 7–20.
- Monaco C, Tortorici L and Paltrinieri W (1998) Structural evolution of the Lucanian Apennines, southern Italy. *Journal of Structural Geology* 20, 617–38.
- Moore CH (2002) Carbonate reservoirs porosity evolution and diagenesis in a sequence stratigraphic framework. *Marine and Petroleum Geology* 19, 1295–6.
- Moore DM and Reynolds Jr RC (1997) *X-ray Diffraction and Identification and Analysis of Clay Minerals*, 2nd edn. Oxford and New York: Oxford University Press, 378 pp.
- Mosca F and Wavrek DA (2002) Petroleum system characteristics of Val d'Agri region, Southern Apennines, Italy (abs.). AAPG ACE.
- Mostardini F and Merlini S (1986) Appennino centro-meridionale. *Sezioni geologiche e proposta di modello strutturale. Memorie della Società Geologica Italiana* 35, 177–202.
- Myers R and Aydin A (2004) The evolution of faults formed by shearing across joint zones in sandstone. *Journal of Structural Geology* 26, 947–66.
- Nelson R (2001) *Geologic Analysis of Naturally Fractured Reservoirs*. Amsterdam: Elsevier, pp. 101–22.
- Noguera AM and Rea G (2000) Deep structure of the Campanian-Lucanian Arc (Southern Apennine, Italy). *Tectonophysics* 324, 239–65.
- Novellino R, Prosser G, Spiess R, Viti C, Agosta F, Tavarnelli E and Bucci F (2015) Dynamic weakening along incipient low-angle normal faults in pelagic limestones (Southern Apennines, Italy). *Journal of the Geological Society* 172, 283–6.
- Nur A and Israel M (1980) The role of heterogeneities in faulting. *Physics of the Earth and Planetary Interiors* 21, 225–36.
- Odling NE, Gillespie P, Bourguin B, Castaing C, Chilés JP, Christensen NP, Fillion E, Genter A, Olsen C, Thrane L, Trice R, Aarseth E, Walsh JJ and Watterson J (1999) Variations in fracture system geometry and their implications for fluid flow in fractured hydrocarbon reservoirs. *Petroleum Geoscience* 5, 373–84.
- Panza E, Agosta F, Rustichelli A, Vinciguerra SC, Ougier-Simonin A, Dobbs M and Prosser G (2019) Meso-to-microscale fracture porosity in tight limestones: results of an integrated field and laboratory study. *Marine and Petroleum Geology* 103, 581–95.
- Panza E, Agosta F, Rustichelli A, Zambrano M, Tondi E, Prosser G, Giorgioni M and Janiseck JM (2016) Fracture stratigraphy and fluid flow properties of shallow-water, tight carbonates: the case study of the Murge Plateau (southern Italy). *Marine and Petroleum Geology* 73, 350–70.
- Panza E, Agosta F, Zambrano M, Tondi E, Prosser G, Giorgioni M, Janiseck JM (2015) Structural architecture and discrete fracture network modelling of layered fractured carbonates (Altamura Fm., Italy). *Italian Journal of Geosciences* 134(3), 409–22.
- Patacca E, Sartori R and Scandone P (1990) Tyrrhenian basin and Apenninic arcs: kinematic relations since Late Tortonian times. *Memorie della Società Geologica Italiana*, 45, 425–51.
- Patacca E and Scandone P (2007) Geology of the Southern Apennines. *Bollettino della Società Geologica Italiana, Supplemento* 7, 75–119.
- Patacca E, Scandone P, Bellatalla M, Perilli N and Santini U (1992a) The Numidian-sand event in the Southern Apennines. *Memorie di Scienze Geologiche già Memorie degli Istituti di Geologia e Mineralogia dell'Università di Padova, all.* 43, 297–337.
- Patacca E, Scandone P, Bellatalla M, Perilli N and Santini U (1992b) La zona di giunzione tra l'arco appenninico settentrionale e l'arco appenninico meridionale nell'Abruzzo e nel Molise. In *Studi preliminari all'acquisizione dati del profilo CROP 11 Civitavecchia-Vasto* (eds M Tozzi, GP Cavinato and M Parotto), AGIP-CNR-ENEL, Studi Geologici Camerti, Vol. Spec. 1991-2, pp. 417–41.
- Perri F, Caracciolo L, Cavalcante F, Corrado S, Critelli S, Muto F and Dominici R (2016) Sedimentary and thermal evolution of the Eocene-Oligocene mudrocks from the southwestern Thrace Basin (NE Greece). *Basin Research* 28, 319–39.
- Petrella E, Aquino D, Fiorillo F and Celico F (2015) The effect of low-permeability fault zones on groundwater flow in a compartmentalized system: experimental evidence from a carbonate aquifer (Southern Italy). *Hydrological Processes* 29, 1577–87.
- Piedilato S and Prosser G (2005) Thrust sequences and evolution of the external sector of a fold and thrust belt: an example from the Southern Apennines (Italy). *Journal of Geodynamics* 39, 386–402.
- Pollard DD and Aydin A (1990) Progress in understanding jointing over the past century. *Special Papers of the Geological Society of America* 253, 313–36.
- Pollastro RM (1993) Consideration and applications of the illite/smectite geothermometer in hydrocarbon-bearing rocks of Miocene to Mississippian age. *Clays and Clay Minerals* 41, 119–33.
- Priest SD and Hudson JA (1981) Estimation of discontinuity spacing and trace length using scanline surveys. *International Journal of Rock Mechanics and Mining Sciences and Geomechanics Abstracts* 18, 183–97.
- Prosser G, Palladino G, Avagliano D, Coraggio F, Bolla EM, Riva M and Catellani DE (2021) Stratigraphic and tectonic setting of the Liguride units

- cropping out along the southeastern side of the Agri Valley (Southern Apennines, Italy). *Geosciences (Switzerland)* **11**, 125.
- Randazzo V, Di Stefano P, Schlagintweit F, Todaro S, Cacciatori MS and Zarcone G** (2021) The migration path of Gondwanian dinosaurs toward Adria: new insights from the Cretaceous of NW Sicily (Italy). *Cretaceous Research* **126**, 104–919.
- Rohrbaugh Jr MB, Dunne WM and Mauldon M** (2002) Estimating fracture trace intensity, density, and mean length using circular scan lines and windows. *AAPG Bulletin* **86**, 2089–2104.
- Romano V, Bigi S, Carnevale F, De'haven Hyman J, Karra S, Valocchi AJ, Tartarello MC, Battaglia M** (2020) Hydraulic characterization of a fault zone from fracture distribution. *Journal of Structural Geology* **135**, 104036.
- Rustichelli A, Tondi E, Agosta F, Cilona A and Giorgioni M** (2012) Development and distribution of bed-parallel compaction bands and pressure solution seams in carbonates (Bolognano Formation, Majella Mountain, Italy). *Journal of Structural Geology* **37**, 181–99.
- Rustichelli A, Tondi E, Korneva I, Baud P, Vinciguerra S, Agosta F, Reuschlé T and Janiseck JM** (2015) Bedding-parallel stylolites in shallow-water limestone successions of the Apulian carbonate platform (central-Southern Italy). *Italian Journal of Geosciences* **134**, 513–34.
- Rustichelli A, Torrieri S, Tondi E, Laurita S, Strauss C, Agosta F and Balsamo F** (2016) Fracture characteristics in Cretaceous platform and overlying ramp carbonates: an outcrop study from Maiella Mountain (central Italy). *Marine and Petroleum Geology* **76**, 68–87.
- Sartoni S and Crescenti U** (1961) Ricerche biostratigrafiche nel Mesozoico dell'Appennino meridionale. *Giornale di Geologia, ser. 2a*, **29**, 161–302.
- Sartoni S and Crescenti U** (1962) *Ricerche biostratigrafiche nel Mesozoico dell'Appennino meridionale*, Bologna: Museo geologico Giovanni Capellini, p 142.
- Schettino A and Turco E** (2011) Tectonic history of the Western Tethys since the Late Triassic. *Bulletin of the Geological Society of America* **123**, 89–105.
- Schöpfer MPJ, Arslan A, Walsh JJ and Childs C** (2011) Reconciliation of contrasting theories for fracture spacing in layered rocks. *Journal of Structural Geology* **33**, 551–65.
- Scrocca D, Carminati E and Doglioni C** (2005) Deep structure of the southern Apennines, Italy: thin-skinned or thick-skinned? *Tectonics* **24**, 1–20.
- Selli R** (1957) Sulla trasgressione del Miocene nell'Italia meridionale. *Giornale di Geologia, ser. 2a*, **26**, 1–54.
- Shiner P, Beccacini A and Mazzoli S** (2004) Thin-skinned versus thick-skinned structural models for Apulian carbonate reservoirs: constraints from the Val d'Agri Fields, S Apennines, Italy. *Marine and Petroleum Geology* **21**, 805–27.
- Smeraglia L, Giuffrida A, Grimaldi S, Pullen A, La Bruna V, Billi A and Agosta F** (2021b) Fault-controlled upwelling of low-T hydrothermal fluids tracked by travertines in a fold-and-thrust belt, Monte Alpi, Southern Apennines, Italy. *Journal of Structural Geology* **144**, 104276.
- Smeraglia L, Mercuri M, Tavani S, Pignalosa A, Kettermann M, Billi A and Carminati E** (2021a) 3D Discrete Fracture Network (DFN) models of damage zone fluid corridors within a reservoir-scale normal fault in carbonates: multiscale approach using field data and UAV imagery. *Marine and Petroleum Geology* **126**, 104902.
- Spalluto L** (2008) Sedimentology and high-resolution sequence stratigraphy of a Lower Cretaceous shallow-water carbonate succession from the western Gargano Promontory (Apulia, Southern Italy). *GeoActa, Special Publication* **1**, 77–96.
- Spalluto L** (2012) Facies evolution and sequence chronostratigraphy of a 'mid'-Cretaceous shallow-water carbonate succession of the Apulia Carbonate Platform from the northern Murge area (Apulia, southern Italy). *Facies* **58**, 17–36.
- Tavani S, Storti F, Lacombe O, Corradetti A, Muñoz JA and Mazzoli S** (2015) A review of deformation pattern templates in foreland basin systems and fold-and-thrust belts: implications for the state of stress in the frontal regions of thrust wedges. *Earth-Science Reviews* **141**, 82–104.
- Todaro S, Di Stefano P, Zarcone G and Randazzo V** (2017) Facies stacking and extinctions across the Triassic–Jurassic boundary in a peritidal succession from western Sicily. *Facies* **63**, 1–21.
- Todaro S, Rigo M, Randazzo V and Di Stefano P** (2018) The end-Triassic mass extinction: a new correlation between extinction events and  $\delta^{13}\text{C}$  fluctuations from a Triassic–Jurassic peritidal succession in western Sicily. *Sedimentary Geology* **368**, 105–13.
- Trecalli A, Spangenberg J, Adatte T, Föllmi KB and Parente M** (2012) Carbonate platform evidence of ocean acidification at the onset of the early Toarcian oceanic anoxic event. *Earth and Planetary Science Letters*, **357–358**, 214–25.
- Tucker ME** (1985) Shallow-marine carbonate facies and facies models. In *Sedimentology: Recent Developments and Applied Aspects* (eds PJ Benchley and BPJ Williams), London: Spec. Publ. Geol. Soc., 18, pp. 147–69.
- Vezzani L, Festa A and Ghisetti FC** (2010) Geology and tectonic evolution of the Central-Southern Apennines, Italy. *Geological Society of America, Special Papers* **469**, 1–58.
- Vinci F, Iannace A, Parente M, Pirmez C, Torrieri S, Giorgioni M** (2017) Early dolomitization in the lower cretaceous shallow-water carbonates of Southern Apennines (Italy): Clues about palaeoclimatic fluctuations in western Tethys. *Sedimentary Geology* **362**, 17–36.
- Volatili T, Zambrano M, Cilona A, Huisman BAH, Rustichelli A, Giorgioni M, Vittori S and Tondi E** (2019) From fracture analysis to flow simulations in fractured carbonates: the case study of the Roman Valley Quarry (Majella Mountain, Italy). *Marine and Petroleum Geology* **100**, 95–110.
- Waliczek M, Machowski G, Poprawa P, Świerczewska A and Więclaw D** (2021) A novel VRo, T<sub>max</sub>, and S indices conversion formula on data from the fold-and-thrust belt of the Western Outer Carpathians (Poland). *International Journal of Coal Geology* **234**, 103672.
- Wennberg OP, Svåná T, Azizzadeh M, Aqrabi AMM, Brockbank P, Lyslo KB and Ogilvie S** (2006) Fracture intensity vs. mechanical stratigraphy in platform top carbonates: The Aquitanian of the Asmari Formation, Khaviz Anticline, Zagros, SW Iran. *Petroleum Geoscience* **12**, 235–45.
- Wignall PB and Bond DPG** (2008) The end-Triassic and Early Jurassic mass extinction records in the British Isles. *Proceedings of the Geologists' Association* **119**(1), 73–84.
- Wu H and Pollard D** (1995) An experimental study of the relationship between joint spacing and layer thickness. *Journal of Structural Geology* **17**, 887–905.
- Zambrano M, Tondi E, Korneva I, Panza E, Agosta F, Janiseck JM, Giorgioni M** (2016). Fracture properties analysis and discrete fracture network modelling of faulted tight limestones, Murge Plateau, Italy. *Italian Journal of Geosciences* **135**(1), 55–67.
- Zarcone G, Petti FM, Cillari A, Di Stefano P, Guzzetta D and Nicosia U** (2010) A possible bridge between Adria and Africa: new palaeobiogeographic and stratigraphic constraints on the Mesozoic palaeogeography of the Central Mediterranean area. *Earth-Science Reviews* **103**, 154–62.